Check for updates

Received: 11 January 2023 | Revised: 11 March 2023

DOI: 10.1002/app.53919

REVIEW

Applied Polymer SCIENCE WILEY

The advances development of proton exchange membrane with high proton conductivity and balanced stability in fuel cells

Peng Wei[1,2] | **Yang Sui**[2] | **Xiaoyu Meng**[2] | **Qiong Zhou**[2]

[1]State Key Laboratory of Tribology, Department of Mechanical Engineering, Tsinghua University, Beijing, China

[2]Department of Materials Science and Engineering, New Energy and Material College, China University of Petroleum-Beijing, Beijing, China

Correspondence
Peng Wei, State Key Laboratory of Tribology, Department of Mechanical Engineering, Tsinghua University, Beijing 100084, China.
Email: weipeng0710@foxmail.com

Qiong Zhou, Department of Materials Science and Engineering, New Energy and Material College, China University of Petroleum-Beijing, Beijing, 102249, China.
Email: zhouqiong_cn@163.com

Funding information
Foundation of the China University of Petroleum, Beijing, Grant/Award Number: 2462020YXZZ019; China National Key Research and Development Plan, Grant/Award Number: 2022YFC2803702

Abstract

In the proton exchange membrane fuel cell, proton exchange membrane (PEM) serves as both the main conductor of protons and the fuel-blocking membrane. Thus, high proton conductivity and excellent stability are expected for PEMs at the same time. According to chemical structure, this review divides PEM into three groups. Recently, high-performance PEM has been made possible by controlling chemical structure, organic–inorganic hybrid composite membranes, and nanofiber composite membranes. One of them, nanofiber composite membranes, is distinguished by long-range order and is capable of achieving both strong proton conductivity with exceptional stability. The high-performance PEM has been accomplished by the presence of an acid-rich layer, acid–base interaction, and proton transport channel in PEMs are also summarized in this paper. We believe that our discussion will help the researcher create high-performance PEM and pave the way for further developments in the field of energy materials as a whole.

KEYWORDS

acid–base interaction, acid-rich layer, balanced proton conductivity and stability, proton exchange membrane, proton transport mechanism

1 | INTRODUCTION

Finding clean, alternative energy sources is crucial because of the major challenge of energy scarcity caused by the growing depletion of fossil fuels. Fuel cells are acknowledged as a crucial technical solution in the context of "carbon peaking" and "carbon neutralization" because they are a successful technique for converting chemical energy into electrical energy.[1,2] Additionally, it may work well with clean energy sources like hydrogen.[3,4] Fuel cells can help with the sustainable development of the energy sector, which is one of the primary areas of study being done at the present, because of their exceptional efficiency and lack of contamination.[5]

Depending on the type of electrolyte they utilize,[2,6] fuel cells can be categorized as proton exchange membrane fuel cells (PEMFC), solid oxide fuel cells (SOFC), and alkaline membrane fuel cells (AMFC). Among them is the PEMFC, which has become one of the energy technologies that is currently used the most around the globe because of its excellent energy conversion and lack of pollutants. PEMFC typically consists of membrane electrode assembly (MEA) and bipolar plates (BPs), with the MEA including the catalyst layer (CL), gas diffusion layer (GDL), and PEM.[7] The fuel travels through BPs to the

 © 2023 Wiley Periodicals LLC.

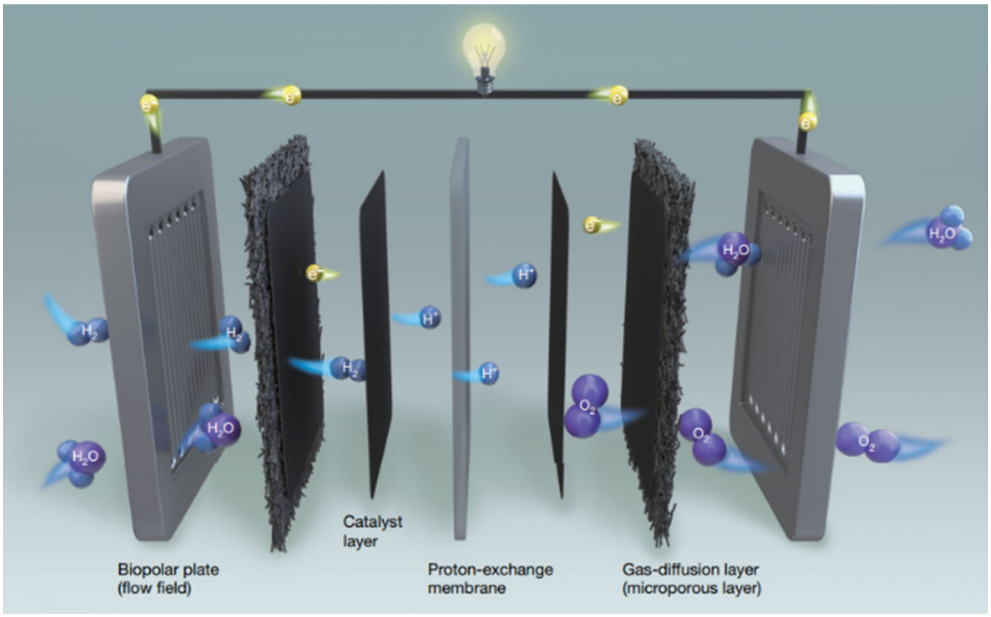


FIGURE 1 The composition and proton conduction principle in PEMFC[8] (reprinted with permission from Ref. 8; copyright (2021) nature). [Color figure can be viewed at wileyonlinelibrary.com]

GDL, where it undergoes oxidation at the anode, producing protons and current. Protons are then conducted to the cathode through PEM, where a reduction reaction takes place to produce water and other products. To generate electrical energy, electrons enter the cathode through an external circuit. The schematic illustration of the hydrogen fuel cell is depicted in Figure 1 using the operating principles of the hydrogen fuel cell as examples.[8]

PEM must be capable of blocking fuel and conducting protons depending on the PEMFC's operating environment. As a consequence, the PEM requirements can be summarized as follows.

1. High proton conductivity,[9] to ensure effective proton conduction from anode to cathode.
2. Robust fuel barrier ability,[10] to prevent fuel penetration and fuel cell performance degradation or even short circuit.
3. Good mechanical characteristics in both dry and wet environments,[11] to guarantee that PEM operates normally while being used.
4. Excellent chemical and thermal stability,[12,13] usable in challenging situations.
5. Low price[14] that can satisfy the requirements of commercial and economic use.
6. Strong durability,[15] which is suitable for long-term usage.

PEM can be classified as perfluorinated sulfonic acid membrane, partially fluorinated sulfonic acid membrane, and non-fluorinated sulfonic acid membrane depending on its application needs and chemical structure.

1. Perfluorinated sulfonic acid membrane (PFSA)[16]

Its chemical stability and proton conductivity are both excellent. Nafion, a DuPont product, is currently performing exceptionally well. A highly hydrophobic fluorocarbon backbone and randomly positioned perfluoro ether side chains that end in sulfonic acid radical comprise the random copolymer known as Nafion. Nafion will generate a special phase separation structure due to hydrophobic and hydrophilic variations between the main and side chains, giving PFSA an excellent proton transport capacity. When water or any solvent is introduced to Nafion, this phase separation process will be considerably amplified.

Despite Nafion having a sizable market share, PFSAs with short-side chains still have very high research and development value. PFSAs like 3 M, SSC made by Dow Chemical, Flemion made by Asahi, and GORE-SELECT made by Gore have comparable main chain structures, there are differences in the side chain's length as well as ion exchange capacity (IEC). Due to its enhanced proton conductivity, PFSA with short-side chains has been the subject of extensive research.[17] However, PFSA has a low glass transition temperature, and the ion clusters created by the sulfonic acid after water absorption begin to lose water at 80°C. Furthermore, the proton conductivity, chemical stability, and mechanical stability all drastically decline above 100°C. However, these shortcomings, in addition to the high fuel permeability as well as high cost that become difficult to reduce, prevent application range of PFSA from being further expanded.[18]

2. Partially fluorinated sulfonic acid membrane

A PEM type known as a partial fluorinated sulfonic acid membrane contains the main chain that is

10974628, 2023, 22, Downloaded from https://onlinelibrary.wiley.com/doi/10.1002/app.53919 by Turkey Cochrane Evidence Aid, Wiley Online Library on [22/05/2025]. See the Terms and Conditions (https://onlinelibrary.wiley.com/terms-and-conditions) on Wiley Online Library for rules of use; OA articles are governed by the applicable Creative Commons License

composited with a perfluorinated or fluorinated structure and a side chain that is replaced by a structure free of fluoride.[17,19] The partly fluorinated sulfonic acid membrane has exceptional chemical stability and performs similarly to PFSA because of the higher bond energy in the C—F bond (460 kJ mol^{-1}) than that in the C—H bond (410 kJ mol^{-1}).[20] The proton conductivity as well as stability of PEMs are unaffected when non-fluoropolymers are employed compared with PFSA, and its cost is also reduced. However, the development goal of large-scale commercial application of partially fluorinated sulfonic acid membranes is constrained due to the complexity of the membrane fabrication process of partially fluorinated sulfonic acid membranes and the lack of environmental friendliness.

3. Non-fluorinated sulfonic acid membrane

The main or side chains of PEM that predominates in non-fluorinated sulfonic acid membranes are aromatic or aliphatic. Sulfonated poly (arylene ether sulfone) (sPAES),[21,22] sulfonated poly (aryl ether ketone sulfone) (SPAEKS),[23] sulfonated polyphenylene oxide (SPPO),[24] sulfonated polyimides (SPIs),[25] with sulfonated poly (ether ether ketone) (SPEEK)[26,27] are now the most used non-fluorinated sulfonic acid membranes. These sulfonated polymers could be generated either through monomer polymerization or polymer sulfonation. This is one of the best favorable approaches to constructing high-performance PEM due to the rigid main chain of all the membranes outlined above as well as their exceptional thermal stability and mechanical stability under 200°C. Since its side chain is sulfonic acid and is directly coupled to the rigid main chain, SPEEK is one of the membranes that best represents the non-fluorinated sulfonic acid membrane. In spite of having a higher fuel barrier capacity and high proton conductivity after being synthesized by polymer sulfonation,[28] SPEEK also has tunable proton conductivity, chemical stability, and thermal stability.[13] The percentage of main chains that contain sulfonic acid across all main chains is the degree of sulfonation (DS) of SPEEK. When the reaction time increased from 4 to 24 h, DS of SPEEK changed from 40.2% to 89.2%, and its proton conductivity changed from 16.4 to 38.6 mS cm^{-1} at ambient temperature and 100% RH. Because it can generate free radicals, which can result in chemical degradation of the membranes, Fenton solution was employed to assess the stability of the membrane. When DS of SPEEK rose, the deterioration time in the Fenton test decreased from 200 to 1 min. As a consequence of the thermogravimetric analysis (TGA), thermal stability can be determined. There are three processes in the degradation of SPEEK, which are the evaporation of the solvent, the breakdown of $—SO_3H$, and the main chain of SPEEK, respectively.[29–31] When more $—SO_3H$ was added into SPEEK as the DS grew, the thermal stability of membranes worsened. In conclusion, thermal stability can also be controlled. The group of Xianfeng Li also succeeded in pilot-scale synthesis and roll-to-roll manufacture of SPEEK membranes, allowing SPEEK to be commercialized.[32]

2 | THE FABRICATION OF HIGH-PERFORMANCE PEM

The goal and greatest challenge of current research are to construct a reliable and effective proton transport channel in PEM in order to develop high-performance PEM. The regulation of chemical structure, organic–inorganic hybrid composite membranes, and nanofiber composite membranes are the key areas of concentration in the creation of high-performance PEM.

2.1 | The regulation of chemical structure in PEM

The proton transport capabilities of PEM will be affected by the size, shape, as well as connectivity of hydrophilic ion clusters. Accordingly, by planning and managing PEM from a synthesis-based approach, ideal performance can be attained.[18] Among these, random copolymers, block copolymers, graft copolymers, and polymer sulfonation can be employed to create PEM with varying ion cluster sizes, shapes, and connections. Take SPEEK and Nafion as an example, its schematic can be found in Figure 2.

1. Random copolymers

The random distribution of its hydrophobic and hydrophilic components gives the random copolymer a more homogeneous shape. Furthermore, the hydrocarbon structure is hydrophobic and the sulfonic acid is reduced in comparison to PFSA, which also creates a greater phase separation structure for the hydrophilic structure. The proton conductivity of the random copolymer is markedly decreased than that of PFSA due to these ion clusters are randomly distributed throughout the hydrophobic domain and there is less connection between them.[18]

The hydrophilic and hydrophobic phase separation in the membrane, which would construct proton transport channels, was described using transmission electron microscope (TEM), and its connectivity was consistent with the size of hydrophilic sections. Higher proton

10974628, 2023, 22, Downloaded from https://onlinelibrary.wiley.com/doi/10.1002/app.53919 by Turkey Cochrane Evidence Aid, Wiley Online Library on [22/05/2025]. See the Terms and Conditions (https://onlinelibrary.wiley.com/terms-and-conditions) on Wiley Online Library for rules of use; OA articles are governed by the applicable Creative Commons License

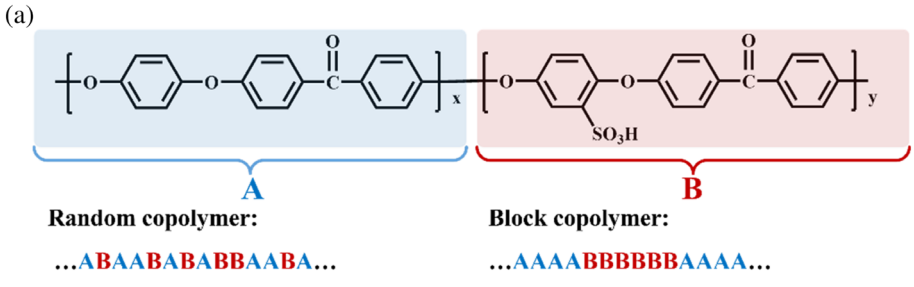


FIGURE 2 The schematic of (a) random copolymer, block copolymer and (b) graft copolymers. [Color figure can be viewed at wileyonlinelibrary.com]

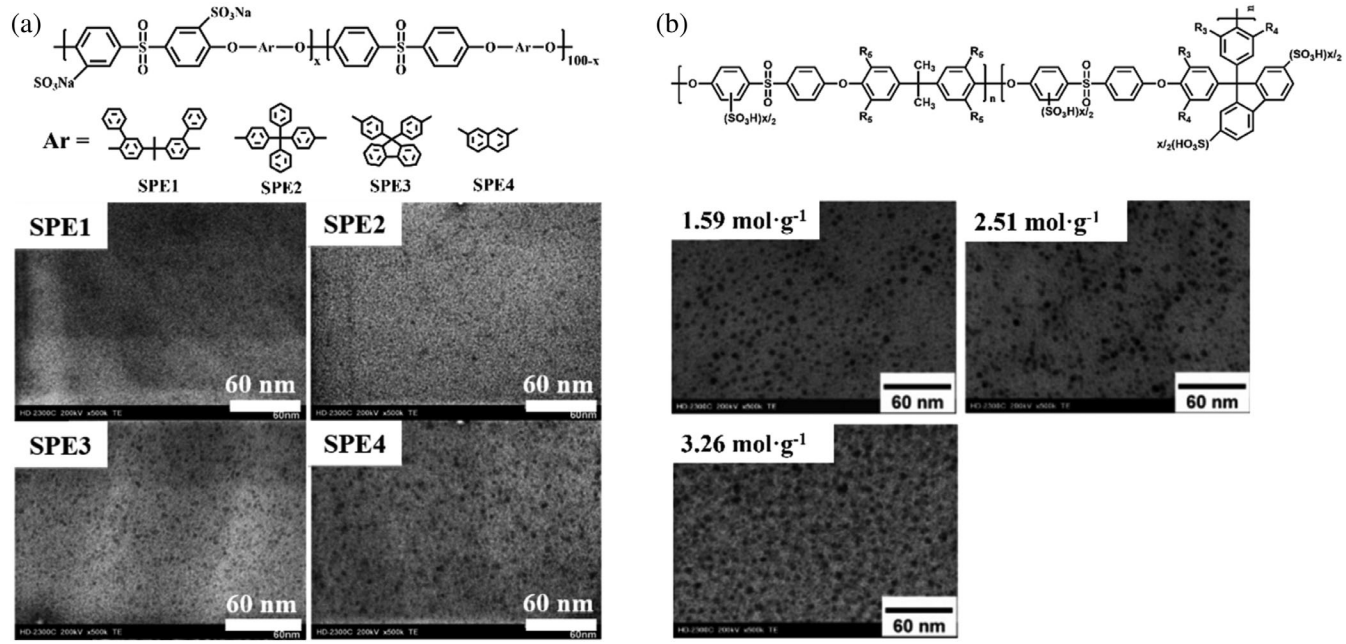


FIGURE 3 The TEM of (a) sulfonated polyether (SPE) random polymers[35] and (b) sulfonated poly (arylene ether sulfone)s with different IECs[36] (reprinted with permission from Refs. 35, 36; copyright (2009) Macromolecules; copyright (2007) Journal of the American Chemical Society).

conductivity is associated with better-connected proton transport channels. In order to explain the rise in proton conductivity, TEM is always used. To enhance the contrast of hydrophilic and hydrophobic area, the membrane always stained with lead acetate. Therefore, the dark area can be ascribed to the hydrophilic regions and bright area can be ascribed to the hydrophobic regions in the TEM.[33,34] By investigating the impact of hydrophobic component size and shape on the randomly copolymerized sulfonated polyether (SPE), Bae et al.[35] discovered that the size or shape of hydrophilic ion clusters increased with the decrease of hydrophobic components, its hydrophilic region was distributed uniformly in the membrane and was shown in Figure 3a. The hydrophilic

10974628, 2023, 22, Downloaded from https://onlinelibrary.wiley.com/doi/10.1002/app.53919 by Turkey Cochrane Evidence Aid, Wiley Online Library on [22/05/2025]. See the Terms and Conditions (https://onlinelibrary.wiley.com/terms-and-conditions) on Wiley Online Library for rules of use; OA articles are governed by the applicable Creative Commons License

portion of a tiny, flat naphthalene structure can be formed by the aggregation of hydrophobic parts. SPE4 membranes with smaller hydrophobic components have lesser water absorption when compared to other membranes with larger hydrophobic components, but their hydrophilic ion clusters have better connections and higher proton conductivity. The hydrophilic area is increasingly larger as the IEC increases,[36] as illustrated in Figure 3b. IEC is one of the key techniques for measuring the degree of sulfonation reaction, which measures the type and number of carriers and their capacity to dissociate protons.[37,38] The higher the IEC, higher content of —SO_3H would be obtained in the main chain of membrane. Moreover, the hydrophilic area of the membrane that includes —SO_3H would be used to construct proton transport channels, leading to a high proton conductivity of the random copolymer. However, the drawbacks of high sulfonation, like the increase in water uptake, swelling ratio, as well as reduction in stability, cannot be ignored.

2. Block copolymers

Block copolymers often include both hydrophilic and hydrophobic structural components, and their sections clearly demonstrate micro-phase separation. The block copolymer's swelling degree exhibits anisotropy due to its distinctive sequence structure. In addition, especially at moderate temperatures or low relative humidity, its proton conductivity may be superior to that of PFSA. Amphiphilic block copolymers are therefore thought to be one of the possible contenders for creating high-performance PEM materials.[18] The structure of the hydrophobic block copolymer created by Badami et al.[39] using a fluoro coupling agent based on sulfonated poly (aryl ether sulfone) (SPAE) was depicted through atomic force microscope (AFM) as shown in Figure 4a. AFM was employed to obtain topographical photographs from the membranes and evaluate their surface roughness. It can characterize the peculiar micro-phase separation structure of the membrane, the hydrophobic backbone nanophase and the hydrophilic ionic nanophase are the bright and dark domains, respectively. Therefore, AFM can further confirm the connected proton transport channels built through the hydrophilic region, which may lead to high proton conductivity. As coupling agents, hexafluorobenzene (HFB) and decafluorobiphenyl (DFBP) were introduced to hydroxyl terminated oligomers, and temperature of coupling reaction was reduced to control the rate at which sulfonated oligomers' chains grew. According to the findings, block copolymers containing HFB and DFBP exhibit good hydrophilicity, as shown in Figure 4a, and both exhibit good hydrophilic and hydrophobic phase separation structures, with the block copolymers containing DFBP having more advantages in phase separation structures. One important element influencing the formation behavior of polymer phase separation morphology is block length of hydrophilic as well as hydrophobic repeating units. As the block length is increased, the hydrophilic area of the proton transport channel will connect better, increasing the proton conductivity.[40] Although the block copolymer's structural layout allows for adjustment of the proton transport channel continuity, the material's potential applications are constrained by the difficult manufacturing procedure.

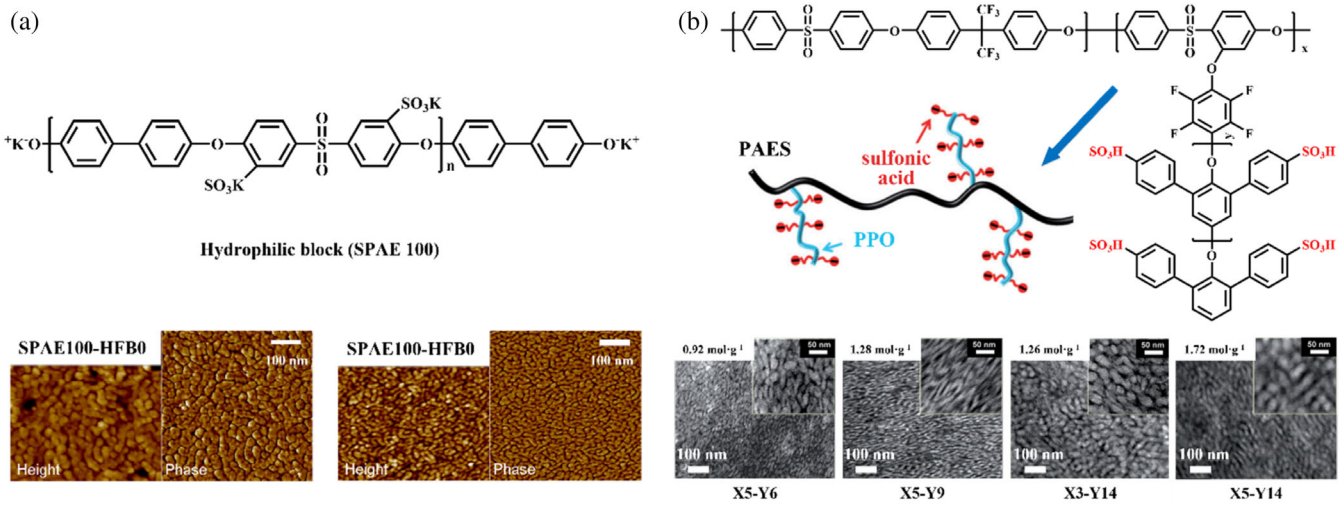


FIGURE 4 (a) AFM on SPAE100-HFB0 and SPAE100-DFPB0,[39] (b) TEM of SPPO side chain grafted PAES with different IEC values[41] (reprinted with permission from Refs. 39, 41; copyright (2009) Journal of Membrane Science; copyright (2011) Angewandte Chemie International Edition). [Color figure can be viewed at wileyonlinelibrary.com]

10974628, 2023, 22, Downloaded from https://onlinelibrary.wiley.com/doi/10.1002/app.53919 by Turkey Cochrane Evidence Aid, Wiley Online Library on [23/05/2025]. See the Terms and Conditions (https://onlinelibrary.wiley.com/terms-and-conditions) on Wiley Online Library for rules of use; OA articles are governed by the applicable Creative Commons License

3. Graft copolymers

To create materials with a hydrophobic structure similar to PFSA, graft copolymers are used to connect hydrophilic aromatic or aliphatic side chains into hydrophobic main chains. Graft copolymers, like block copolymers, can easily produce phase-separation structures and they are more connected since they are composed of parts with conducting and non-conducting protons. By modifying the side chain's structure and length, it is possible to modify the graft copolymer's shape and, in turn, alter the proton transport channel and hydrophilic ion cluster sizes to achieve the desired properties.[18] To create the graft copolymer depicted in Figure 4b, Li et al.[41] grafted the side chain of poly aryl ether sulfone (PAES) onto the side chain of SPPO. The polymer's side chain features sulfonic acid groups with comb structures, which clearly demonstrate a phase separation structure. Its hydrophilic region is made up of ion clusters that are linked to each other and have a structure like PFSA. During the 30%–90% RH range, the proton conductivity of these four membranes (X5-Y6, X5-Y9, X3-Y14, and X5-Y14) ranged from 10^{-2} to more than 10^{-1} S·cm^{-1}. Regardless of the minimum IEC values, their proton conductivities were higher or comparable than that of Nafion 112.

4. Polymer sulfonation

All of the aforementioned random, block and graft copolymers were produced by polymerizing monomers. The preparation procedure is rather complicated, and phase separation of PEM is regulated by the structure's design. By sulfonating PEEK in strong sulfuric acid, PEM manufactured through the sulfonation method, such as SPEEK, is created.[13] The structure of SPEEK, which comprises a hydrophobic main chain as well as a hydrophilic side chain, is comparable to that of a graft copolymer. Simply adjusting the composite membrane's sulfonation duration and degree will produce SPEEK with the requisite proton conductivity and stability.[13,42,43] It has been one of the areas of current research because this process feature indicates that it is simple to mass produce and has a big potential to replace Nafion in commercialization.[44]

2.2 | Organic–inorganic hybrid composite membranes

By building a connected proton transport channel in PEM and lowering the energy needed for proton transport, high-performance PEM can be generated. By doping the PEM matrix with nanoparticles that facilitate proton transport, the organic–inorganic hybrid[45] approach can produce proton transport channels, lower activation energy, as well as ultimately enhance proton conductivity of the composite membrane. The following two categories are based on whether the doped nanoparticles conduct protons.

1. Non-proton conducting nanoparticles

Zirconia (ZrO_2),[46] titanium dioxide (TiO_2),[31,47–50] carbon nanotubes,[51,52] and other non-conducting nanoparticles typically require to exhibit hydrophilicity, as do nanoparticles with distinctive morphologies like porous,[46] columnar,[31] lamella,[53,54] spherical,[55–57] and so on. The stability of PEM is unaffected. These nanoparticles can assist with more water retention and connect to the proton transport channel in PEM, enhancing proton conductivity.

As illustrated in Figure 5a,b, Matos et al.[55] modified the Nafion matrix by adding spherical TiO_2 (TP25), mesoporous TiO_2 (TMP), and nanotube TiO_2 (TNT). Small angle X-ray scattering (SAXS) was then applied to assess microstructure of the composite membrane. The Bragg equation is used to determine the size of ion cluster in the membrane, and the calculation outcomes are depicted in Figure 5c. It was discovered that the size of ion clusters would vary depending on whether these membranes were dry or wet. In the wet film, the size of the three ion clusters following the addition of TNT is significantly larger than that of other composite membranes, however, in the dry film, the size of the three ion clusters is essentially the same. The maximum water absorption and best performance are found in the composite membrane containing TNT, proving that inorganic fillers' ability to absorb and retain water can enhance the connectivity of proton transport channels in PEM and be crucial to high-performance PEM. The water absorption and hygroscopicity of the non-proton conducting nanoparticles only slightly improve the connection and proton conductivity of PEM. Typically, nanoparticles that can conduct protons themselves or interact with the polymer matrix to assist conduction are added to the polymer matrix in order to further boost proton conductivity.

2. Proton conducting nanoparticles

This type of nanoparticle is a material that either possesses proton conductivity on its own or can interact with the polymer matrix after addition, allowing proton transmission. Of all conductive nanoparticles, heteropoly acid is the most typical. It is thought to be a powerful proton conductor due to its unusual structure and strong acidity. For example, phosphotungstic acid (HPW),[58–60] silicotungstic acid (HSiW),[61] and so forth, have the common formula $[XM_{12}O_{40}]^{n-}$ (where X = P, Si, Ge, etc., and M = Mo, W, etc.). In HPW, the Keggin structure, which has 12 co-edge metal oxygen octahedrons (WO_6)

10974628, 2023, 22, Downloaded from https://onlinelibrary.wiley.com/doi/10.1002/app.53919 by Turkey Cochrane Evidence Aid, Wiley Online Library on [22/05/2025]. See the Terms and Conditions (https://onlinelibrary.wiley.com/terms-and-conditions) on Wiley Online Library for rules of use; OA articles are governed by the applicable Creative Commons License

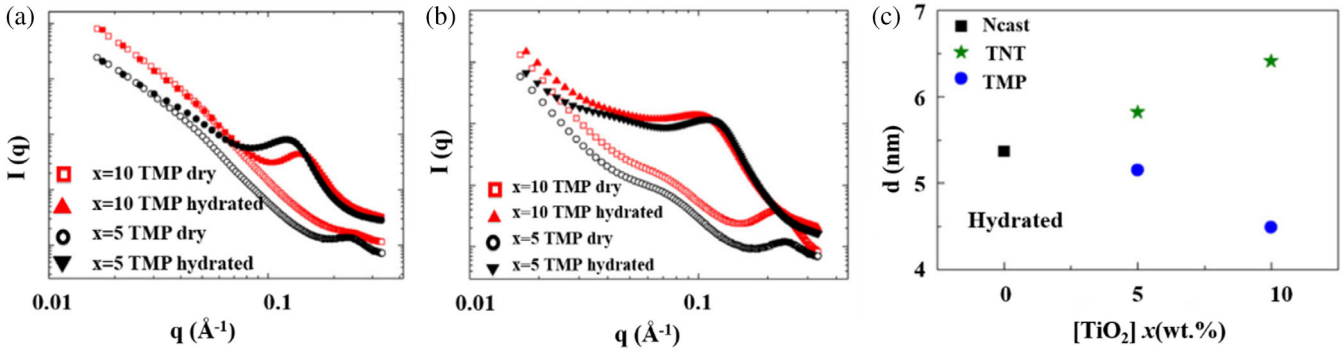


FIGURE 5 The SAXS of composite membranes with (a) mesoporous titania and (b) titania nanotubes, and (c) its size of ionic clusters in the hydrated state[55] (reprinted with permission from Ref. 55; copyright (2011) Journal of Power Sources). [Color figure can be viewed at wileyonlinelibrary.com]

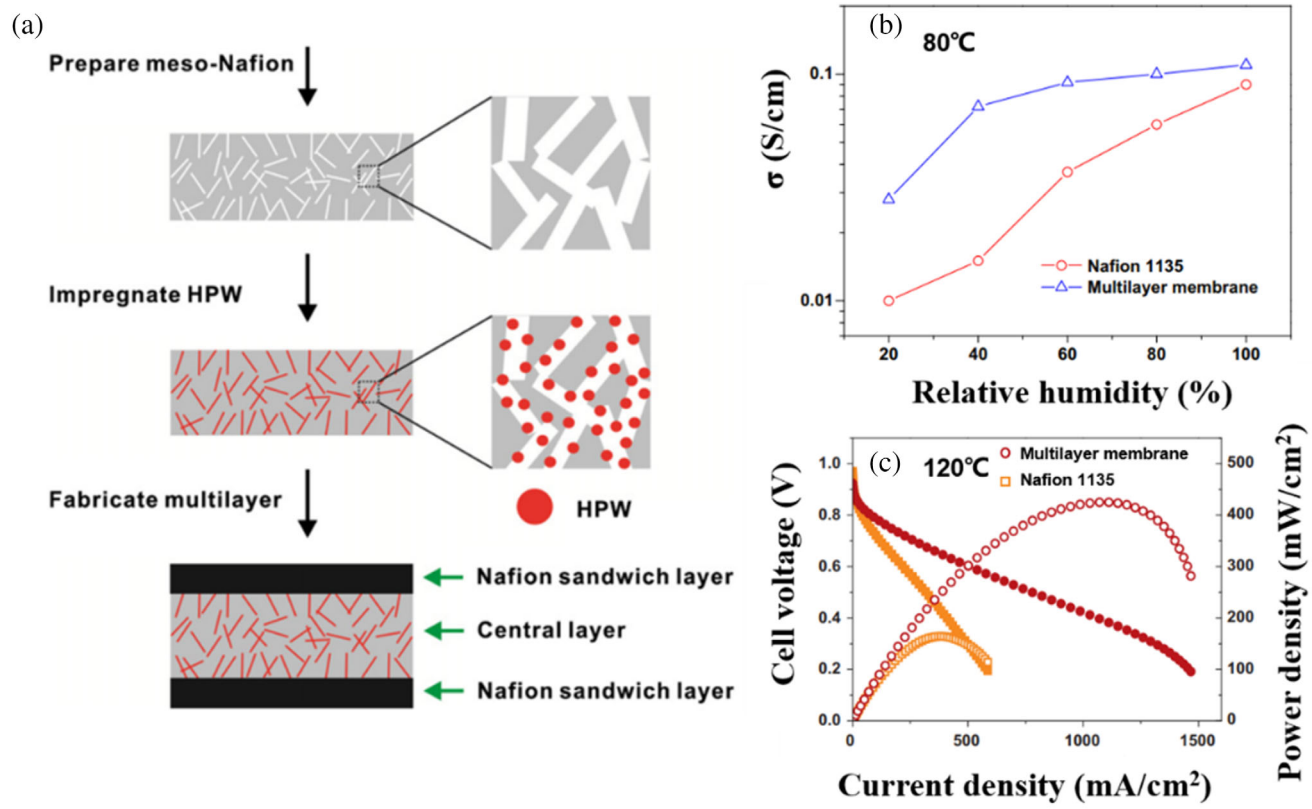


FIGURE 6 (a) Schematic diagram of the preparation of multilayer membrane based on Nafion, (b) its proton conductivity, and (c) fuel cell performance[64] (reprinted with permission from Ref. 64; copyright (2013) Journal of Membrane Science). [Color figure can be viewed at wileyonlinelibrary.com]

encircling the central phosphorus (P) atom of tetrahedral coordination, serves as an example of the unit. Acidic protons that are isolated from one another directly exist on polyanions. Water then dissolves these protons to create protonated water molecules (H_3O^+ and $H_5O_2^+$). However, solitary protons can move quickly between nearby polyanions and are the reason for severe acidity. Additionally, even at ambient temperature, they have a significant intrinsic proton conductivity of 0.02–0.1 $S{\cdot}cm^{-1}$.[62,63] As displayed in Figure 6a, Lu et al.[64] constructed a porous Nafion matrix, submerged it in HPW solution, and then sealed the membrane's upper and lower ends with Nafion. The proton conductivity of the membrane, which is 0.072 $S{\cdot}cm^{-1}$ under 80°C and 40% RH, is four times greater than Nafion 1135 under the same condition. According to Figure 6b,c, the fuel cell

10974628, 2023, 22, Downloaded from https://onlinelibrary.wiley.com/doi/10.1002/app.53919 by Turkey Cochrane Evidence Aid, Wiley Online Library on [22/05/2025]. See the Terms and Conditions (https://onlinelibrary.wiley.com/terms-and-conditions) on Wiley Online Library for rules of use; OA articles are governed by the applicable Creative Commons License

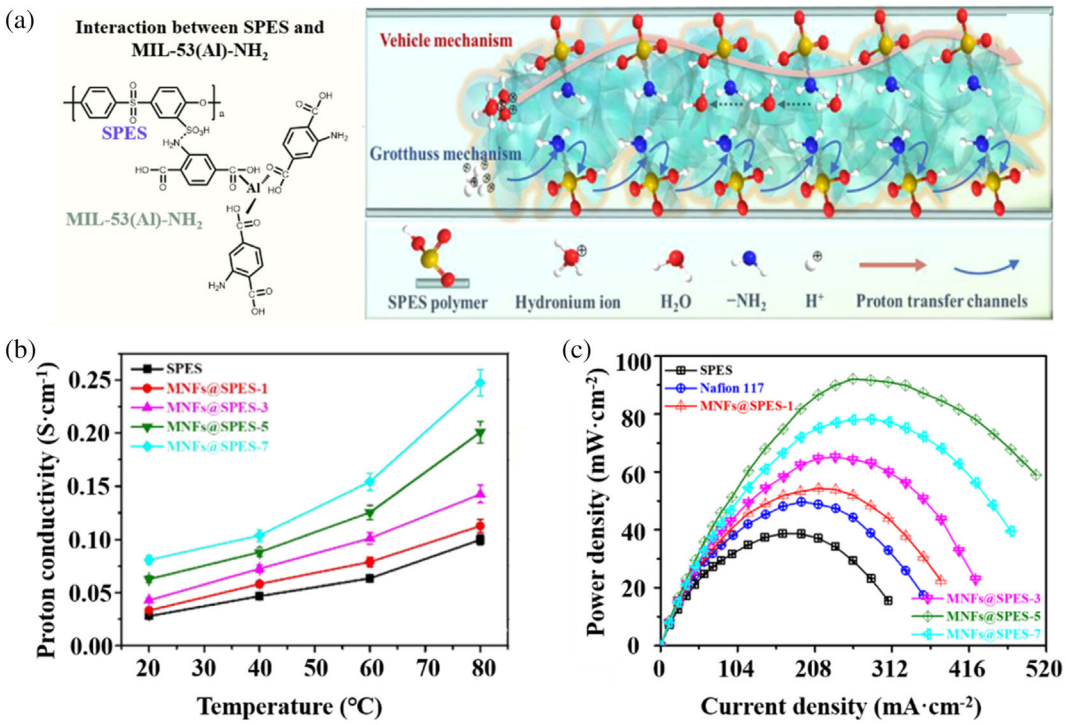


FIGURE 7 The schematic of the proton transport mechanism, (b) proton conductivity, and (c) fuel cell performance of the MNFs@SPES composite membranes[80] (reprinted with permission from Ref. 80; copyright (2019) ACS Applied Materials & Interfaces). [Color figure can be viewed at wileyonlinelibrary.com]

performance of these membranes at 120°C is 420 mW·cm^{-2}, 2.5 times that of Nafion 1135 under the identical situations. The main problem of the composite membrane with HPW has evolved as a result of the high water solubility of HPW and the tease of separation from PEM, which causes a drop in proton conductivity.[65] Additionally, the nanoparticles with adaptable structures and groups include metal–organic frameworks (MOF),[66,67] covalent organic frameworks (COF),[68–70] graphene (Gra)[71,72] and structures that are similar to graphene (such as MoS_2[73,74] and g-C_3N_4[75–78]) can be used in PEM. Taking MOF as an example, it is a porous crystal material formed by self-assembly after metal ions/clusters coordinate with organic connectors.[79]

The MNFs@SPES composite membrane was fabricated by Wang et al.[80] by introducing MIL-53(Al)-NH_2(MNF) to the sulfonated polyethersulfone (SPES) polymer. Its schematic illustration of the transmission procedure is displayed in Figure 7a. MNF with a high specific surface area can construct a long-range ordered proton transport channel in the SPES matrix, which is advantageous for the proton to conduct. Its conductivity of MNFs@SPES-7 is 0.248 S·cm^{-1} at 80°C and 100% RH, 2.5 times that of pure SPES under the same circumstances. Excellent fuel cell property is obtained by the MNFs@SPES membrane in methanol fuel cells. Among these, the power density of MNFs@SPES-5 reaches 92.063 mW cm^{-2}, which is 85.4% higher than that of Nafion 117 and 137.8% larger than that of pristine SPES membrane under the identical situations as displayed in Figure 7b,c.

Usually, two or more proton-conductive nanoparticles are employed in high-performance PEM. The evolution of research on organic–inorganic hybrid composite membranes during the previous few years is summarized in Table 1.

Under an applied electric field of 500 V/cm, Swati et al.[84] employed sulfonated carbon nanotubes (s-CNTs) oriented in SPEEK through electrophoretic effect to transform the original short-range linked s-CNTs into long-range connected ones, as illustrated in Figure 8a,b. As demonstrated in Figure 8c, S-sCNT-5 membrane has a proton conductivity of 43.1 mS cm^{-1} at 30°C, which is significantly greater than that of SPEEK. As shown in Figure 8d, Zhao[48] produced long-range ordered nanoparticles by orienting TiO_2 in an electric field ranging from 0–4000 V/cm; at room temperature and 100% RH, the proton conductivity of SPEEK/TiO_2-15% changed from 4.8 to 8.5 mS cm^{-1}. The proton conductivity of SPEEK/TiO_2-15% was 4.84 mS cm^{-1} at 23°C and 100% RH under 4000 V/cm, which was 75% higher than casting method. Additionally, Fang[85] employed sulfonated graphene nanosheets (sGNP)

10974628, 2023, 22, Downloaded from https://onlinelibrary.wiley.com/doi/10.1002/app.53919 by Turkey Cochrane Evidence Aid, Wiley Online Library on [22/05/2025]. See the Terms and Conditions (https://onlinelibrary.wiley.com/terms-and-conditions) on Wiley Online Library for rules of use; OA articles are governed by the applicable Creative Commons License

TABLE 1 The research progress of organic–inorganic hybrid membranes.

Morphology	Polymer	Nanoparticles	Temperature (°C)	Humidity (%)	Proton conductivity ($mS \cdot cm^{-1}$)	Ref.
Lamella	SPEEK	g-C_3N_4 + HPW	20	100	86	65
Column	SPEEK	imidazole-functionalized halloysite nanotubes (mHNT) + HPW	25	95	71	81
Porous	Nafion	ZIF8@GO	80	40	210	66
	SPEEK	S-UiO66@GO	70	95	268	28
	SPEEK	ZIF-8 + CNT	120	30	50	82
	SPEEK	HPW@MIL-101	60	100	272	83

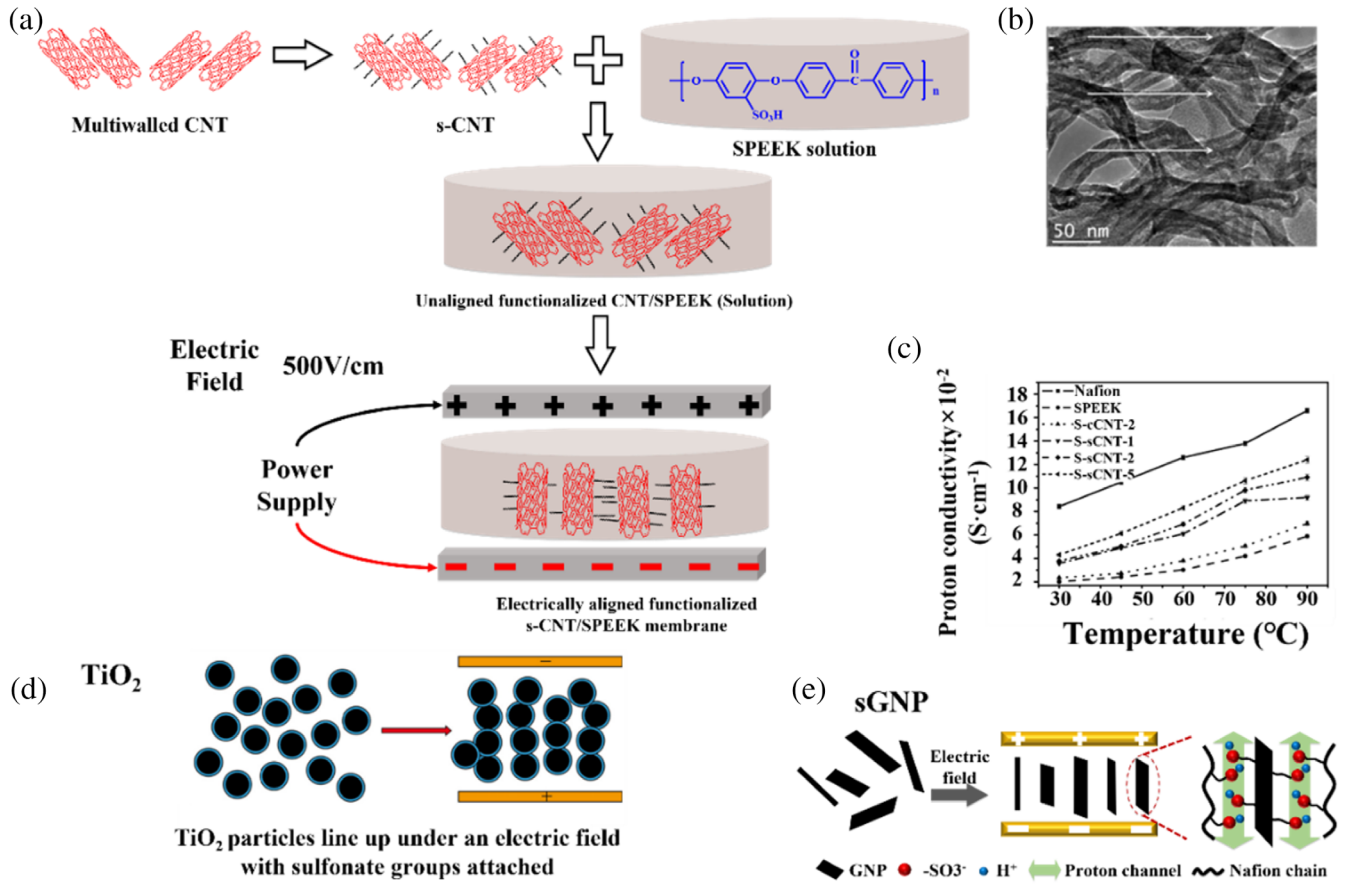


FIGURE 8 (a) The schematic illustration of the preparation of s-CNT/SPEEK composite membranes under electric field, (b) its TEM and (c) proton conductivity,[84] the ordered arrangement of (d) TiO_2[48] and (e) sGNPs under electric field[85] (reprinted with permission from Refs. 48, 84, 85; copyright (2015) ACS Applied Materials & Interfaces; copyright (2013) Journal of Membrane Science; copyright (2021) International Journal of Hydrogen Energy). [Color figure can be viewed at wileyonlinelibrary.com]

as illustrated in Figure 7e, which altered the proton conductivity of SPEEK/sGNP-0.5% from 95 to 110 mS cm^{-1} at 50°C and 100% RH. The value for SPEEK/sGNP-0.5% was 155 mS cm^{-1} at 80°C and 100% RH under 4000 V/cm, which was 48% higher than the value for Nafion produced using the conventional casting approach.

In light of this, Liu et al.[86,87] coupled HPW (w/w = 1/3) with the ferrocyanide-coordinated poly (4-vinylpyridine) (CP4VP) to create the novel Fe-C-C-W structure depicted in Figure 9a. The aforementioned proton-conducting component (PC) is added to polysulfone (PSf) to create a long-range connectivity structure under the influence of a magnetic field with a 35-tesla field exerted, as illustrated in Figure 9b. According to Figure 9c, contrast the TEM images of composite membranes with (MMs-PC) and without (NMs-PC) magnetic fields. It is discovered that it is similar to that of an electric field, meaning that as the proton conduction component content increases, the short-range

10974628, 2023, 22, Downloaded from https://onlinelibrary.wiley.com/doi/10.1002/app.53919 by Turkey Cochrane Evidence Aid, Wiley Online Library on [22/05/2025]. See the Terms and Conditions (https://onlinelibrary.wiley.com/terms-and-conditions) on Wiley Online Library for rules of use; OA articles are governed by the applicable Creative Commons License

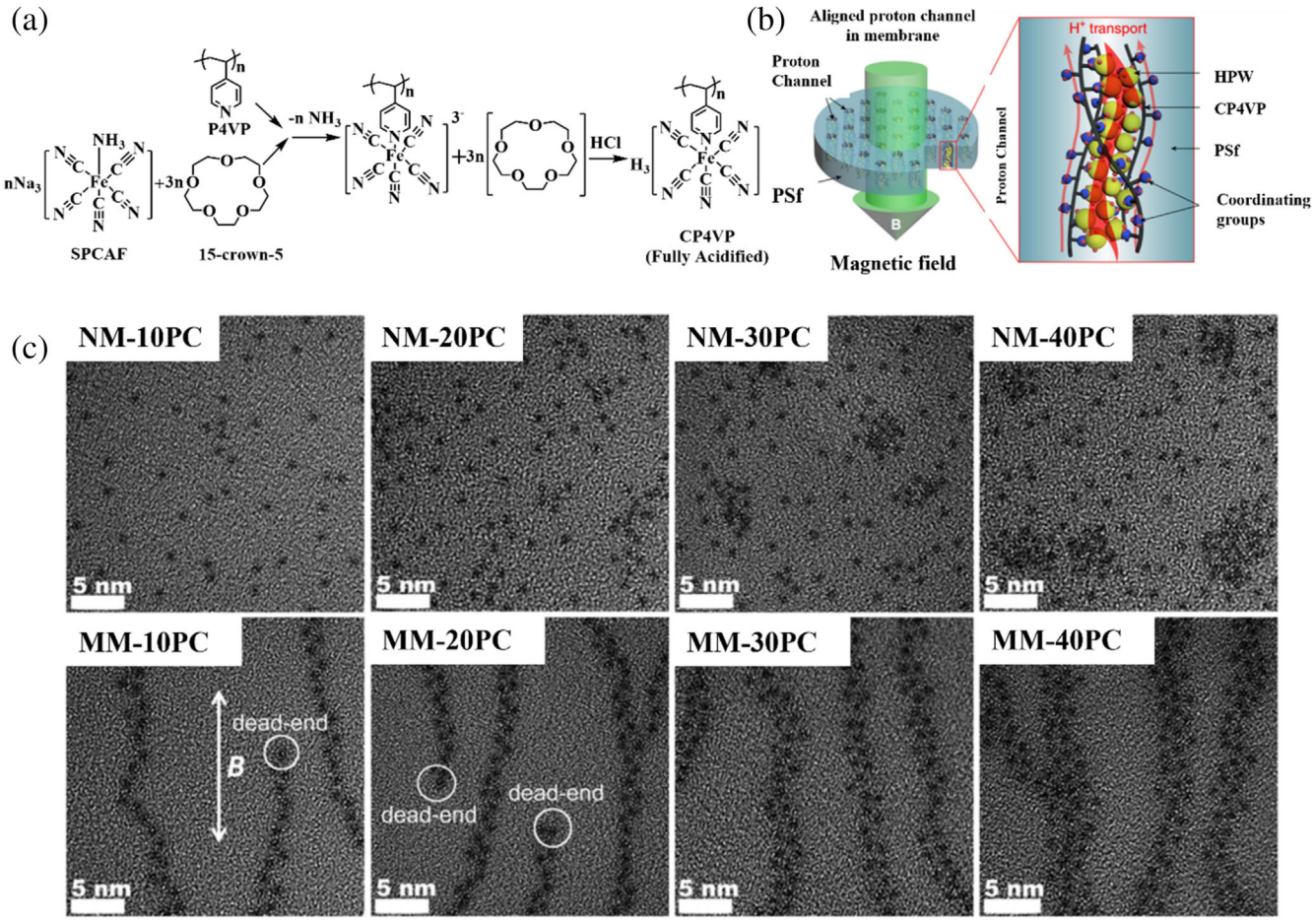


FIGURE 9 (a) The synthesis route of CP4VP and (b) its schematic and (c) TEM with HPW under the magnetic field to form ordered arrangement[86,87] (reprinted with permission from Refs. 86, 87; copyright (2020) Energy & Environmental Science; copyright (2019) Nature Communications). [Color figure can be viewed at wileyonlinelibrary.com]

connected filler transforms into a long-range ordered filler under the influence of the magnetic field, resulting in preparation of the high-performance membrane.

Nanoparticles require the application of electric[48,84,85] or magnetic fields[86–89] in order to construct long-range ordered proton transport channels. Their mechanical characteristics and proton conductivity will be reduced due to their complex procedure and agglomeration issues, which will impair their performance. Long-term order is a property of the nanofiber. As a result, the PEM made from nanofiber can not only address the issue of nanoparticles being unable to link over long distances but also prevent the agglomeration of nanoparticles. It is the ideal method for preparing high-performance PEM.

2.3 | Nanofiber composite membranes

To construct the nanofiber composite membrane, functionalized or unfunctionalized nanofibers are added toward the polymer matrix. High strength and simple functionalization are the main features of nanofibers.[5,90–92] They serve as a network of support and can conduct protons, balancing high proton conductivity and excellent stability. As can be seen in Figure 10a,b, Wang et al.[93] prepared composite membranes with an excellent performance by adding micron cellulose fibers to a Nafion solution. In the hydrogen/air fuel cell test, the composite membranes' optimum power density under 80°C is 23 mW cm^{-2}, as illustrated in Figure 10c. To construct nanofiber composite membranes, Zhang et al.[94] developed sulfonated poly (aryl ether sulfone ketone) (SPPESK) nanofibers with an average diameter of about 120 nm by electrospinning as displayed in Figure 11. The proton conductivity, swelling stability, mechanical stability, and thermal stability of these composite membranes with nanofibers are noticeably better than those of the pristine SPPESK membrane. The proton conductivity is 1.3 times greater than that of ordinary casting membranes.

10974628, 2023, 22, Downloaded from https://onlinelibrary.wiley.com/doi/10.1002/app.53919 by Turkey Cochrane Evidence Aid, Wiley Online Library on [22/05/2025]. See the Terms and Conditions (https://onlinelibrary.wiley.com/terms-and-conditions) on Wiley Online Library for rules of use; OA articles are governed by the applicable Creative Commons License

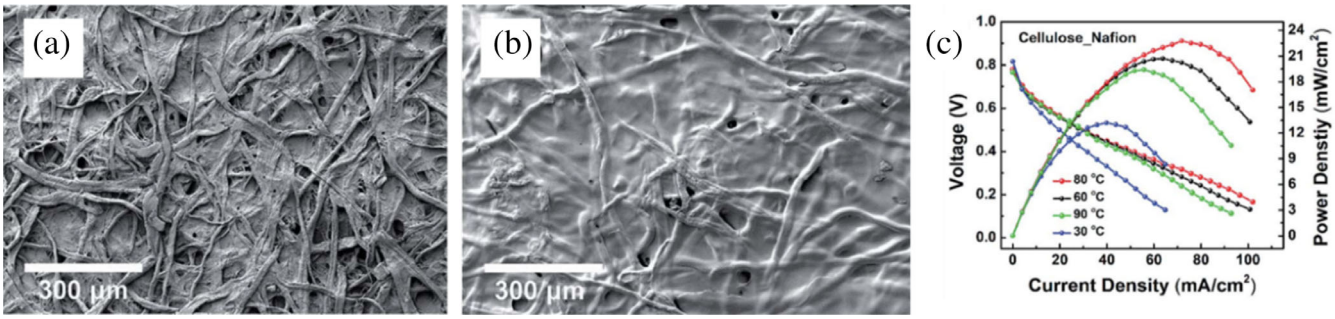


FIGURE 10 The scanning electron microscope (SEM) of (a) cellulose and (b) cellulose/Nafion membrane, and (c) its H_2/Air fuel cell performance[93] (reprinted with permission from Ref. 93; copyright (2019) Sustainable Energy & Fuels). [Color figure can be viewed at wileyonlinelibrary.com]

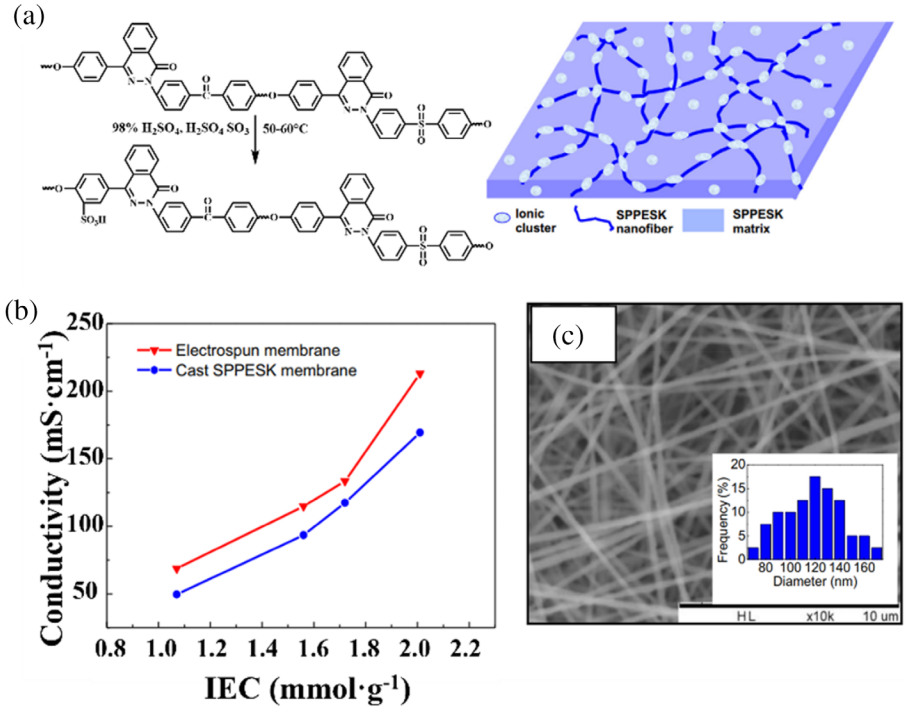


FIGURE 11 (a) The schematic of fabrication SPPESK and SPPESK nanofiber composite membrane and (b) its proton conductivity, (c) the SEM of SPPESK nanofibers and its distribution[94] (reprinted with permission from Ref. 94; copyright (2015) Journal of Membrane Science). [Color figure can be viewed at wileyonlinelibrary.com]

Comparatively, it is discovered that electrospinning is a superior technique for building proton transport channels in PEM because it can generate nanoscale nanofibers with high controllability and a significant amount of specific surface area.[95,96] Below is a summary of the procedures and techniques used to create high-performance nanofiber composite membranes using electrospinning technology. The goal of electrospinning technology is to increase the voltage between the grounding collector and the polymer so that the electrostatic force acting on the liquid polymer at the needle tube's tip can produce a nanofiber. As the electric field strength increases, the droplet's hemispherical surface will expand to create a cone known as a Taylor cone.[92] The solution jet emerges from the tip of the Taylor cone when the electric field attains a critical strength and releases the surface tension of the liquid drop. The solvent eventually evaporates and solidifies to create a continuous nanofiber felt as its jets fly to the collector. The specific surface area of the electrospinning is large. A continuous and stable proton transport channel that is beneficial for proton transport can be created by composing with the polymer at the interface between the polymer and the nanofiber.[97] Additionally, the use of nanofiber can help the composite membrane remain stable in high-temperature, high-humidity environments, prevent swelling, and aid in fuel blockage.[98] Nanofibers make up for the shortcoming of the long-range connectivity of nanoparticles. When compared to non-proton conducting nanoparticles, nanofibers have the advantage of directly conducting protons or interacting with the matrix to improve the proton transmission efficiency, which can simultaneously meet the

10974628, 2023, 22, Downloaded from https://onlinelibrary.wiley.com/doi/10.1002/app.53919 by Turkey Cochrane Evidence Aid, Wiley Online Library on [22/05/2025]. See the Terms and Conditions (https://onlinelibrary.wiley.com/terms-and-conditions) on Wiley Online Library for rules of use; OA articles are governed by the applicable Creative Commons License

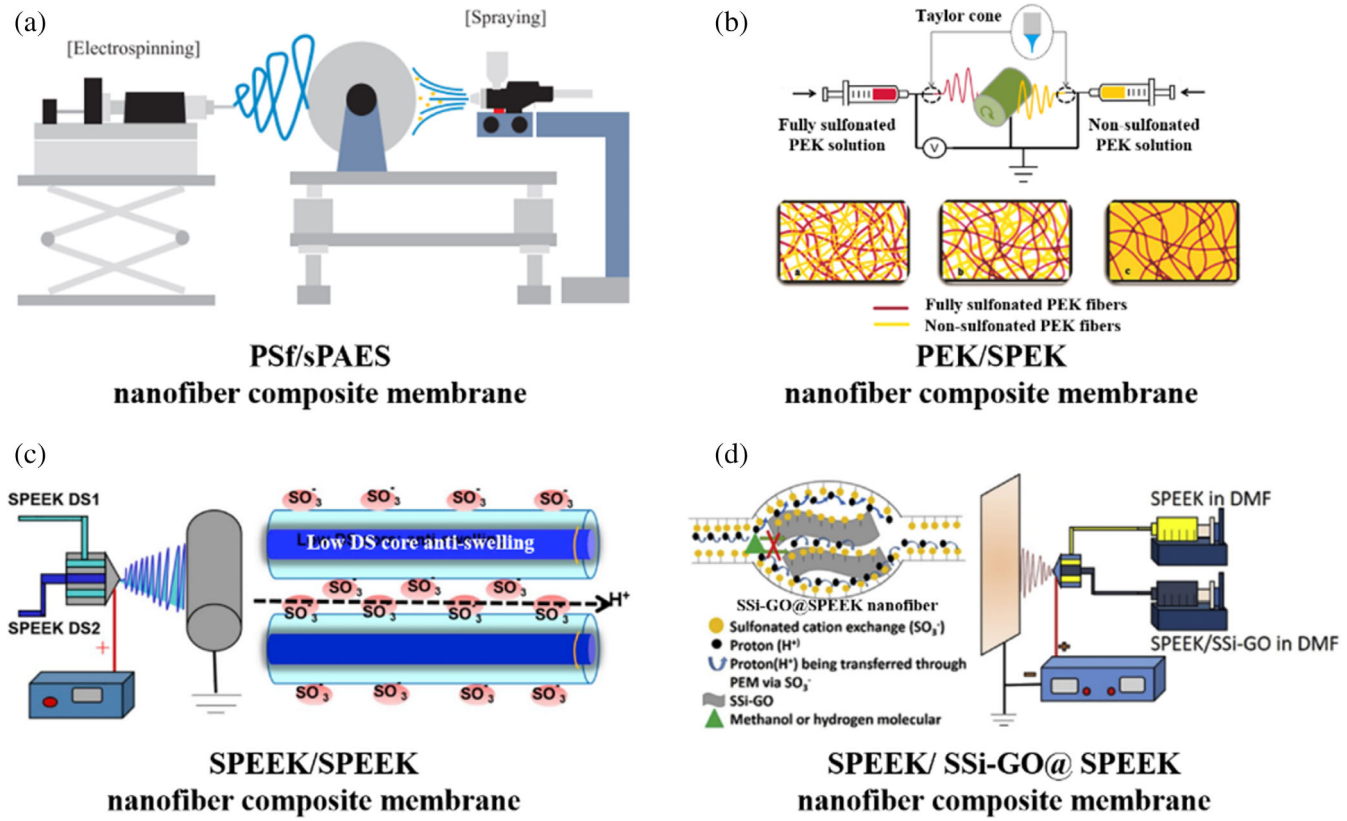


FIGURE 12 The nanofiber composite membranes fabricated by hot pressing method: (a)PSf nanofiber/sPAES,[21] (b)PEK nanofiber/SPEK,[102] (c)SPEEK nanofiber/SPEEK[103] and (d) SPEEK nanofiber/SSi-GO@SPEEK[104] composite membrane (reprinted with permission from Refs. 21, 102–104; copyright (2018) Journal of Membrane Science; copyright (2015) Chemical Engineering Journal; copyright (2020) Journal of Membrane Science; copyright (2019) International Journal of Hydrogen Energy). [Color figure can be viewed at wileyonlinelibrary.com]

demands of strong conductivity and excellent stability of composite membranes. In contrast to the organic–inorganic hybrid composite membrane's solvent-casting approach, a hot-pressing technique can also be used to create nanofiber composite membranes.[99,100]

1. Nanofiber composite membrane fabricated through hot-pressing

First, the nanofibers are prepared by electrospinning. Then, under the circumstances of hot pressing, the difference in glass transition temperature (Tg) between polymers[101] is used to hot press nanofibers and nanofibers or nanofibers and polymers. In this procedure, nanofibers or polymers with lower Tg are inserted into the gap of nanofibers with high Tg to create a dense composite layer under high temperature and pressure. Following are the precise techniques.

As seen in Figure 12a, Jang et al.[21] carried out electrospraying (SP) on sPAES and electrospinning (ES) on PSf. Finally, hot pressing was used to create the membrane. The IEC of the membrane will be decreased after addition of pure sPAES, and its proton conductivity will fall to 0.0763 S cm^{-1} as opposed to 0.116 S·cm^{-1}, because PSf does not have a proton conducting the group. It is made into a double-layer nanofiber mat utilizing the technology of simultaneous electrospinning of poly (ether ketone) (PEK) and sulfonated poly (ether ketone) (SPEK) by Oroujzadeh et al.[102] The nanofiber mat is compressed and hot pressed to create a composite membrane using the two materials' different glass transition temperatures ($Tg_{PEK} = 159°C$, $Tg_{SPEK} = 250°C$) as displayed in Figure 12b. Coaxial spinning was used by He and colleagues to create SPEEK nanofibers with various levels of sulfonation, and then hot pressing was used to create SPEEK composite membranes with various levels of core-shell sulfonation.[103] As illustrated in Figure 12c,d, they also fabricated SSi GO/SPEEK composite membrane[104] that has the same degree of sulfonation but SPEEK in the core contains sulfonated organosilane functionalized graphene oxide nanosheet (SSi-GO). This process creates a hot-pressed nanofiber composite membrane with more ion clusters and a better microphase separation structure than the solvent-casting membrane,

10974628, 2023, 22, Downloaded from https://onlinelibrary.wiley.com/doi/10.1002/app.53919 by Turkey Cochrane Evidence Aid, Wiley Online Library on [22/05/2025]. See the Terms and Conditions (https://onlinelibrary.wiley.com/terms-and-conditions) on Wiley Online Library for rules of use; OA articles are governed by the applicable Creative Commons License

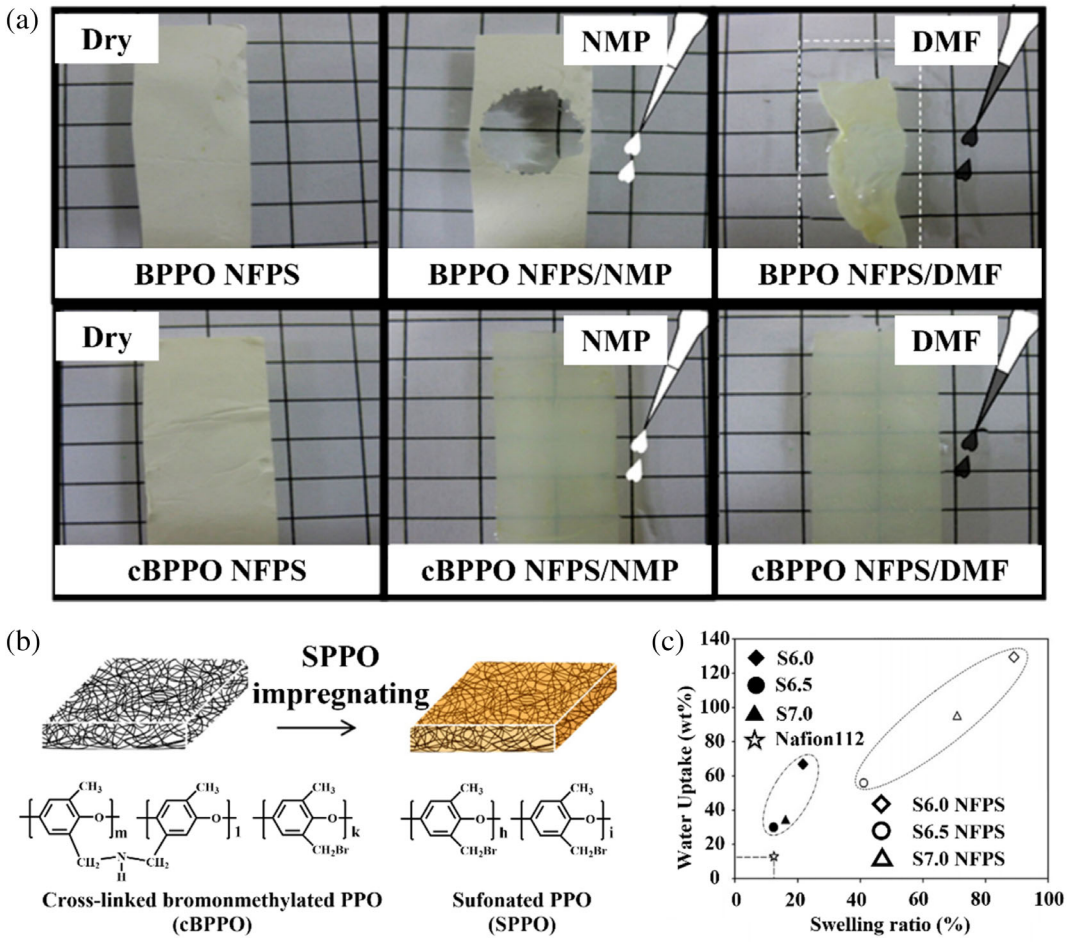


FIGURE 13 (a) The solvent test of cBPPO nanofibers, (b) the membrane composite with SPPO and (c) its water uptake and swelling ratio[24] (reprinted with permission from Ref. 24; copyright (2018) Journal of Membrane Science. [Color figure can be viewed at wileyonlinelibrary.com]

which is better for proton transport. Even while the hot pressing film forming method may successfully create a high-performance composite membrane, it necessitates intricate procedures and great precision, making the casting membrane forming method the most used one at the moment.

2. Nanofiber composite membrane fabricated through solvent-casting

The procedure for forming a casting membrane is straightforward. Nanofibers only need to be added throughout the fabricating process, where they perform a supportive function.[105] Simultaneously, certain functional groups of nanofibers or loaded functional substances may also interact with polymer matrix, enhancing the composite membrane's proton transfer rate and proton conductivity.[105,106]

Bromomethylated polyphenylene oxide (BPPO) nanofiber was fabricated through electrospinning, then put into an ammonia solution for crosslinking by Yun et al.[24] Then, crosslinked bromomethylated poly (2,6-dimethyl-1,4-phenyl ether) (cBPPO) was combined with SPPO matrix to create the composite membrane as shown in Figure 13a. The solvent resistance and stability of cBPPO are excellent. The composite membrane's swelling can be successfully controlled by its organic coupling with the SPPO matrix. After water absorption, the composite membrane's swelling ratio drops from 90% to 20%. However, as illustrated in Figure 13b,c, the addition of nanofiber will also decrease the composite membrane's capacity to absorb water, lowering its proton conductivity.

Li et al.[107] created the 1, 3, and 5 sandwich PVDF/Nafion nanofiber composite membranes to better regulate the position of nanofiber within the polymer by adding polyvinylidene fluoride (PVDF) into the Nafion matrix after spinning. PVDF has excellent chemical, mechanical, and thermal stability and is hydrophobic, which helps it efficiently reduce swelling in PVDF/Nafion composite membranes. However, proton conductivity of composite membranes will decrease as nanofiber content rises.

10974628, 2023, 22, Downloaded from https://onlinelibrary.wiley.com/doi/10.1002/app.53919 by Turkey Cochrane Evidence Aid, Wiley Online Library on [22/05/2025]. See the Terms and Conditions (https://onlinelibrary.wiley.com/terms-and-conditions) on Wiley Online Library for rules of use; OA articles are governed by the applicable Creative Commons License

The interface between the nanofiber and the composite membrane can be increased, and correspondingly the proton conductivity, to further boost performance of the composite membrane. Liu et al.[108] made the SPEEK/PDA@PVDF composite membrane by coating polydopamine (PDA) on the PVDF nanofibers made by electrospinning and adding it to the SPEEK cosolvent, as illustrated in Figure 14a. The membrane is more stable and can prevent fuel from penetrating because of the superior mechanical properties of PVDF. The proton conductivity of the composite membrane under 80°C is 0.06 S/cm as a result of relationship between nanofibers and matrix, which is only marginally less than that of commercial Nafion 115. Zhao et al.[109] created the P/ZIF-8@Nafon composite membrane by growing a layer of ZIF-8 nanoparticles upon that surface of polyisophthalamide nanofibers (PMIA NF), and then filling the pores of the nanofibers with Nafion solution, as illustrated in Figure 14b.

Currently, the acid-rich layer at boundary and acid–base relationship between nanofibers and matrix are the major factors responsible for the capacity of nanofibers to add polymer matrix to enhance the performance of the membrane. The following discussion of these two mechanisms is meant to serve as a theoretical guide for further investigation.

3 | THE PROGRESS IN THE PROTON TRANSPORT MECHANISM

3.1 | Acid-rich layer in the nanofiber composite membrane

Due to hydrogen bonding interaction, an acid-rich layer can form at the interface when nanofibers are added to the polymer matrix. Moreover, the acid-rich layer can be detected through TEM.[90,110,111] As we can see, the Nafion matrix was infused with phytic acid (Phy) doped polybenzimidazole nanofiber (PBINf) by Tanaka et al.[112] As illustrated in Figure 15a, TEM can be used to observe creation of an acid-rich layer in Nafion matrix and PBI nanofiber. The SPPESK

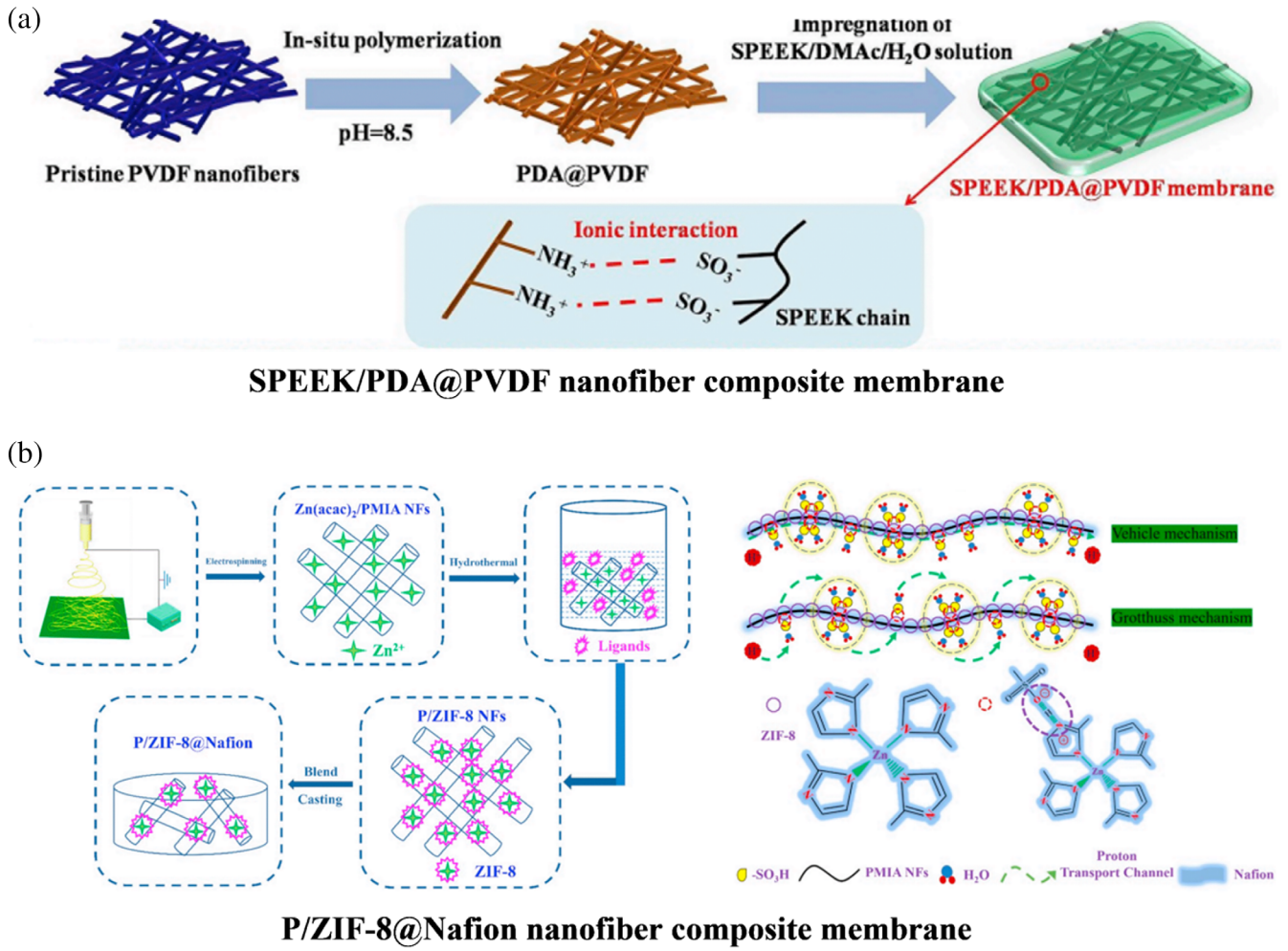


FIGURE 14 The schematic and the interaction of nanofiber composite membranes: (a) SPEEK/PDA@PVDF,[108] (b)P/ZIF-8@Nafion[109] (reprinted with permission from Refs. 108, 109; copyright (2018) Journal of Membrane Science; copyright (2020) Journal of Membrane Science). [Color figure can be viewed at wileyonlinelibrary.com]

10974628, 2023, 22, Downloaded from https://onlinelibrary.wiley.com/doi/10.1002/app.53919 by Turkey Cochrane Evidence Aid, Wiley Online Library on [22/05/2025]. See the Terms and Conditions (https://onlinelibrary.wiley.com/terms-and-conditions) on Wiley Online Library for rules of use; OA articles are governed by the applicable Creative Commons License

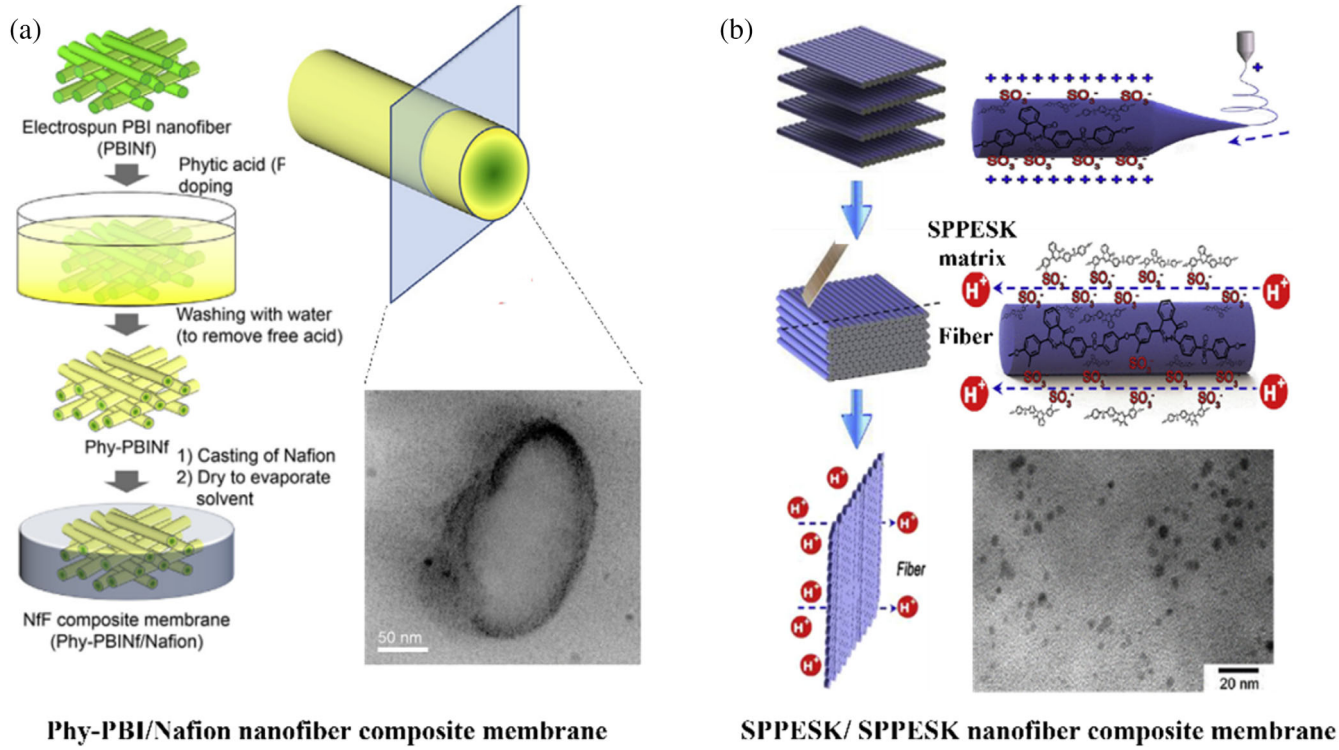


FIGURE 15 The fabrication diagram and TEM of nanofiber composite membranes: (a) Phy-PBI/Nafion,[112] (b) SPPESK/SPPESK[113] (reprinted with permission from Refs. 112, 113; copyright (2017) Journal of Power Sources; copyright (2017) Journal of Power Sources). [Color figure can be viewed at wileyonlinelibrary.com]

nanofiber composite membrane with orderly thickness direction was created by Gong et al.[113] by cutting the ordered SPPESK nanofibers produced by electrospinning into multilayer cubes ($4.5 \times 4.5 \times 2\ cm^3$) and then pouring SPPESK solution on top of it as displayed in Figure 15b.

Zirconium sulfophenylphosphonate (ZrSPP) was added by Ogawa et al.[114] to SPES matrix to create composite membranes. Nuclear magnetic resonance spectroscopy (NMR) and Fourier transform infrared spectroscopy (FTIR) were used to verify the presence of an acid-rich layer at the boundary between ZrSPP and SPES (NRM). Based on the ab-initio method, the proton transport mechanism of the acid-rich layer at boundary was investigated. It was discovered that the hydrogen in the acid-rich layer exhibits less pseudo-shuttle and the hydrogen bond created is weaker, which favors proton transport. The explanation for how the acid-rich layer can increase the composite membrane's proton conductivity is given in Figure 16.

3.2 | Acid–base interaction in the composite membrane

Additionally to the presence of an acid-rich layer in PEM, the layer can build an acid–base interaction that lowers the activation energy of proton conduction in PEM, boosting the proton conductivity of the membrane.[10,97,109,115] According to Figure 17, Wang et al.[116] combined electrospun SPEEK nanofiber with chitosan (CS) matrix, causing an acid–base interaction along the nanofiber direction between —SO_3H in SPEEK and —NH_2 on CS. On the one hand, it can restrict chain movement, provide thermal stability and structural stability for the composite membrane, enhance mechanical qualities, and lessen swelling. The presence of acid–base pairs, on the other hand, can lower activation energy of proton conduction, which is advantageous for proton transport and increases conductivity of the membrane. Zhao et al.[117] functionalized polyacrylonitrile (PAN) nanofibers with L-arginine to create A/PAN nanofibers, which were then combined with a sulfonated polysulfone (SPSF) matrix to create composite membranes. The activation energy of proton conduction in the membrane is decreased by formation of acid–base pairs between amino acid in arginine on A/PAN nanofiber and the sulfonic acid in SPSF matrix, effectively increasing conductivity of the membrane to 0.216 S/cm under 80°C and 100% RH.

According to the principles of density functional theory, Chen et al.[70] first created the neutral COF (TAP-COF), polar COF (PD-COF), Lewis alkaline COF (DAAQ-COF), and positively charged COF (EB-COF), and then added phosphoric acid (PA) to these four

10974628, 2023, 22, Downloaded from https://onlinelibrary.wiley.com/doi/10.1002/app.53919 by Turkey Cochrane Evidence Aid, Wiley Online Library on [22/05/2025]. See the Terms and Conditions (https://onlinelibrary.wiley.com/terms-and-conditions) on Wiley Online Library for rules of use; OA articles are governed by the applicable Creative Commons License

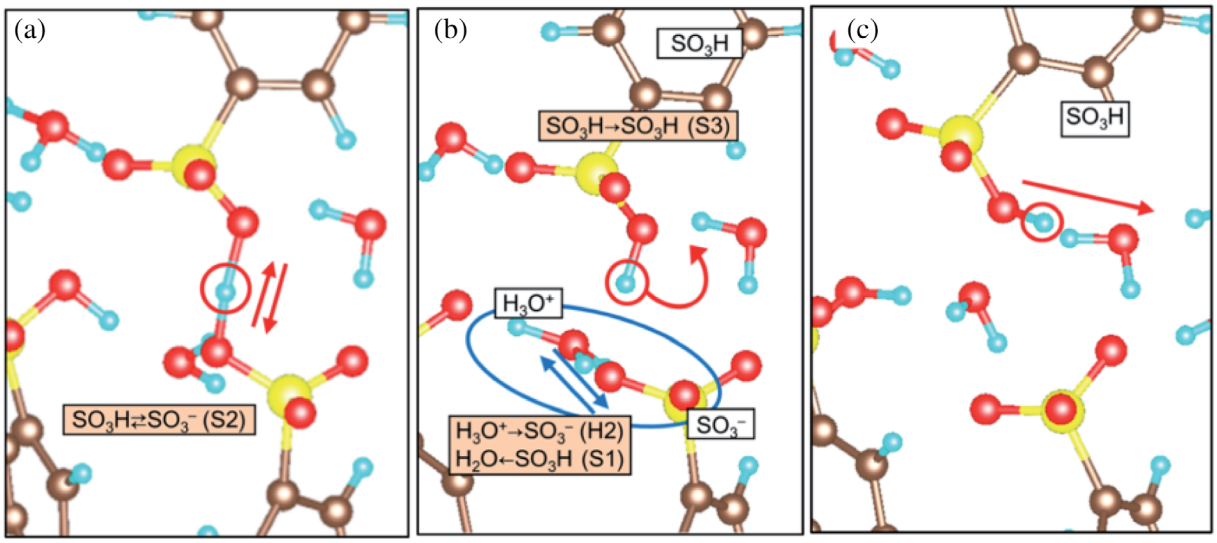


FIGURE 16 The proton conduction mechanism of ZrSPP/SPES composite membrane[114] (reprinted with permission from Ref. 114; copyright (2017) Chemical Science). [Color figure can be viewed at wileyonlinelibrary.com]

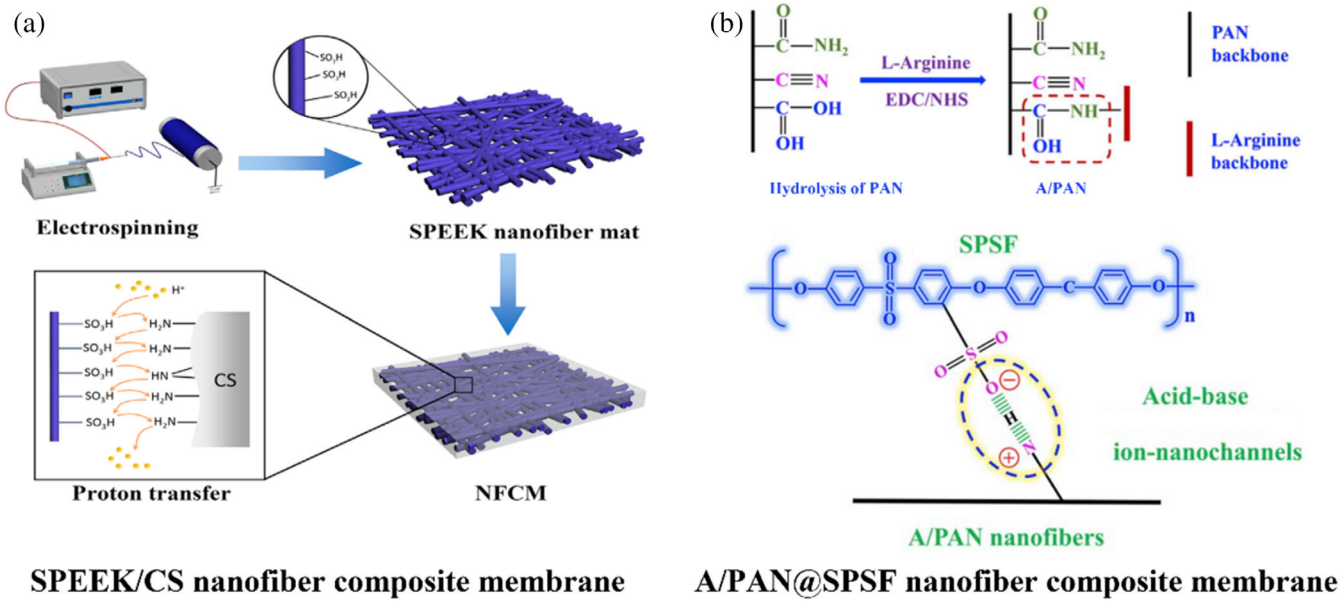


FIGURE 17 The schematic of construction method of continuous nanofiber composite membrane and its acid–base interaction: (a) SPEEK/CS,[116] (b) A/PAN@SPSF[117] (reprinted with permission from Refs. 116, 117; copyright (2015) Journal of Membrane Science; copyright (2020) Journal of Power Sources). [Color figure can be viewed at wileyonlinelibrary.com]

COFs, as illustrated in Figure 18a,b. According to Figure 18c, the outcomes demonstrate that energy of a proton released by PA drops from 3.86 eV to 3.68, 3.17, 2.89, and 2.38 eV, demonstrating that the existence of acid–base relationship can greatly lower activation energy. Since acid–base relationship (COF···H H_2PO_4) between diphosphate anion and COF skeleton, protons are more readily liberated from PA. The presence of acid–base interaction lowers activation energy of protons, making proton transport easier, and thus improving proton conductivity.

3.3 | The proton transport channels in the proton exchange membrane

Along with the acid-rich layer and the acid–base interaction, the proton transport channel significantly affects the proton

10974628, 2023, 22, Downloaded from https://onlinelibrary.wiley.com/doi/10.1002/app.53919 by Turkey Cochrane Evidence Aid, Wiley Online Library on [22/05/2025]. See the Terms and Conditions (https://onlinelibrary.wiley.com/terms-and-conditions) on Wiley Online Library for rules of use; OA articles are governed by the applicable Creative Commons License

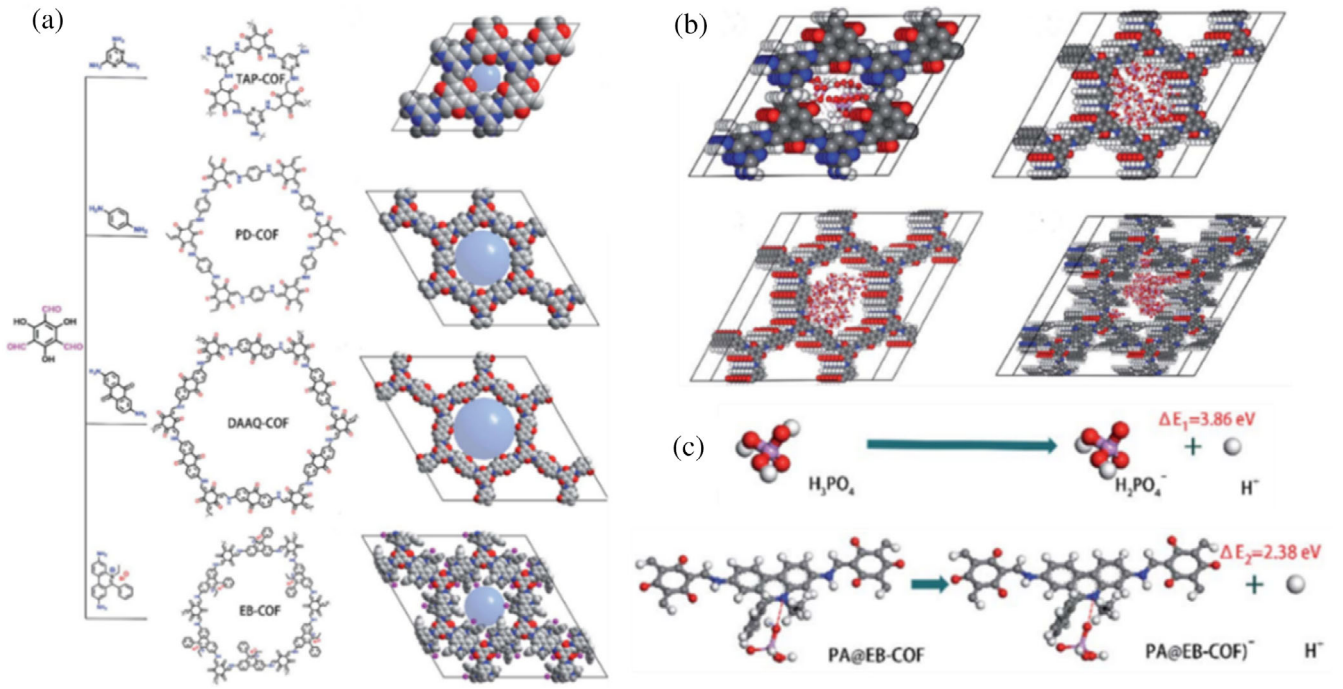


FIGURE 18 (a) The schematic of the fabrication method of four kinds of COF and (b) the addition of PA, (c) activation energy for PA to release proton[70] (reprinted with permission from Ref. 70; copyright (2020) Journal of Materials Chemistry A). [Color figure can be viewed at wileyonlinelibrary.com]

transportation in PEM. The non-fluorosulfonic acid membrane has a poorer conductivity and less favorable dimensional stability when compared to Nafion in PFSA and SPEEK in a PFSA membrane, despite the fact that their IEC values are comparable. This is a result of SPEEK having reduced hydrophobicity of the acid and polymer main chains as well as weaker phase separation between hydrophobicity and hydrophobicity, which causes poor microphase separation effect and even "dead end" phenomena.[118]

Therefore, understanding PEM's microstructure is essential to producing high conductivity, high stability PEM. Hydrophobic main chains as well as hydrophilic side chains make up majority of PEM. This particular arrangement will create a phase separation structure that is favorable for proton conduction,[119] as shown in Figure 19. According to its molecular structure, Nafion has more side chain flexibility than SPEEK, and its hydrophilic region is made up of a reverse micelle structure.[120] When the water content is minimal, as in Figure 19a, the Nafion-formed spherical ion clusters will be evenly dispersed throughout the polymer. The scattered spherical structures will be simpler to link to form a columnar structure as the water content rises. However, the backbone of SPEEK is more rigid, and gaps between the backbone are simple to construct. Spherical and core-shell ion clusters are the most prevalent types of ion clusters in SPEEK, according to SANS and SAXS.[121] Compared to Nafion's, these ion clusters are more distributed and are mostly found in the spaces between the SPEEK main chain. To link and form a proton transport channel, they must take in more water. A higher IEC value, or more ion clusters, are therefore required for SPEEK to have the same high conductivity compared with Nafion. Additionally, as the water concentration rises, the ion cluster is initially surrounded by water before progressively forming a linked polymer sheet. However, if the water content is too high, the proton transmission channel will collapse instead, making proton transmission difficult and lowering the proton conductivity of PEM, as displayed in Figure 19b. In order to connect the spherical or lamellar hydrophilic group ions and create a stable and continuous proton transport channel as well as increase conductivity, the water content will be increased on the assumption that the proton transport channel will not be harmed.

3.4 | The mechanism in the proton exchange membrane

3.4.1 | Proton transport mechanism

Further exploration of proton transportation in PEM and the mechanism of proton transport in PEM are of guiding significance for the preparation of high-performance PEM. Through the channel created through phase separation of hydrophilic and hydrophobic molecules,

10974628, 2023, 22, Downloaded from https://onlinelibrary.wiley.com/doi/10.1002/app.53919 by Turkey Cochrane Evidence Aid, Wiley Online Library on [22/05/2025]. See the Terms and Conditions (https://onlinelibrary.wiley.com/terms-and-conditions) on Wiley Online Library for rules of use; OA articles are governed by the applicable Creative Commons License

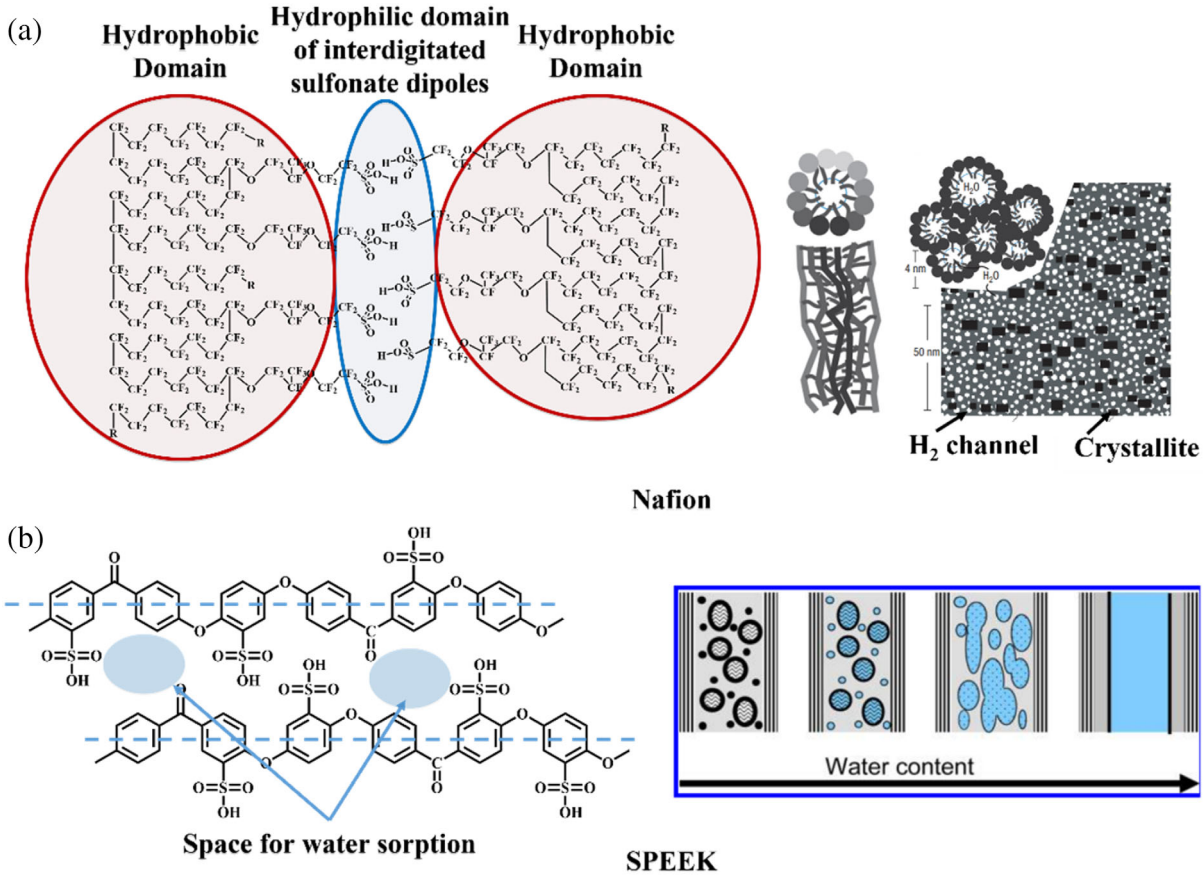


FIGURE 19 The proton transport channel in (a) Nafion[119120] and (b) SPEEK[121] (reprinted with permission from Refs. 119–121; copyright (2020) Journal of Polymer Science Part B; copyright (2008) Nature Materials; copyright (2013) Macromolecules). [Color figure can be viewed at wileyonlinelibrary.com]

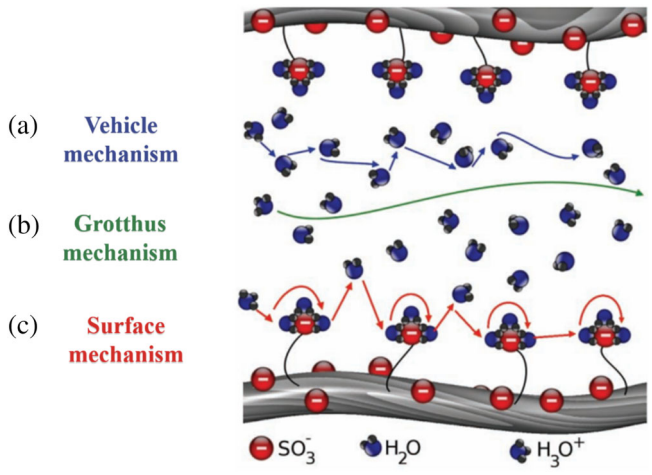


FIGURE 20 The (a) vehicle mechanism, (b) Grotthuss mechanism and (c) surface mechanism in the PEM[123] (reprinted with permission from Ref. 123; copyright (2020) Journal of the Electrochemical Society). [Color figure can be viewed at wileyonlinelibrary.com]

protons are transported in PEM. Currently, it is thought that the primary vehicle, Grotthus, and surface mechanisms[122] are responsible for protons being transmitted in PEM as shown in Figure 20.

Among these, the mobility of hydrated hydrogen ions can be considered as the vehicle mechanism.[124] In PEM, protons travel in the transmission channel as H_3O^+, $H_5O_2^+$, and $H_9O_4^+$ ions. Protons can also be transported by structural diffusion, or the Grotthus mechanism, in contrast to other cations. Protons are "transferred" from one water molecule to another by production and fracture of O—H, and primary carriers of the transfer are $H_5O_2^+$ and $H_9O_4^+$.[125] Protons and anions work together to create a third proton transport mechanism in the PEM, known as the surface transport mechanism. According to this process, protons move between SO_3H and PEM, although this movement takes more activation energy. The vehicle mechanism and Grotthus mechanism are prevalent in PEM when water content is high.[126] In PEM, the surface mechanism takes control of conduction

10974628, 2023, 22, Downloaded from https://onlinelibrary.wiley.com/doi/10.1002/app.53919 by Turkey Cochrane Evidence Aid, Wiley Online Library on [22/05/2025]. See the Terms and Conditions (https://onlinelibrary.wiley.com/terms-and-conditions) on Wiley Online Library for rules of use; OA articles are governed by the applicable Creative Commons License

TABLE 2 The failure mechanism of PEM.

Membranes	Failure mechanism	Operating conditions	Results	Ref.
NU6@PPNF-SPEEK	Chemical degradation	Fenton reagent test during 24 h at 60°C	Dissolved, the peroxyl or hydroxyl radical attact the main chain of SPEEK	105
PI/SPEEK/PI	Chemical degradation	Fenton reagent test during 24 h at 60°C	Dissolved, the peroxyl or hydroxyl radical attact the main chain of SPEEK	90
40%-OPBI	Chemical degradation	Fenton reagent test during 120 h at 80°C	Remains 82.3% weight, PBI membranes with exceptional oxidative stability are preferred to achieve excellent durability	131
SBPI-1.0	Chemical degradation	Fenton reagent test during 12 h at 80°C	Maintains 90% of the initial weight, SBPI has exceptional oxidative stability	132
SPAEK/GO/g-C_3N_4	Chemical degradation	Fenton reagent test during 1 h at 80°C	Maintains 96% of the initial weight, double-filler compositing can enhance the anti-oxidation capability of SPAEK	78
Nafion 211	Mechanical degradation	Cyclic uniaxial tension at controlled temperature and relative humidity	PFSA fatigue would have strong relationship between stress, temperature, and relative humidity, high temperatures reduced fatigue lift significantly than that humidity	133
Nafion 211	Mechanical degradation	Accelerated stress test and In situ crack propagation rates are quantified	The dimensional change of the membrane is highly sensitive to humidity	134
Nafion 211	Mechanical degradation	Elastic–plastic constitutive model compared with cyclic mechanical loadings	Fluctuating humidity load can be more damaging than a fluctuating temperature load, and a minor increase in humidity amplitude can result in a considerable decrease in membrane lifetime.	135
HPW-ILs@MOF4	Thermal degradation	Samples were heated at a rate of 10°C/min in a nitrogen environment.	The breakdown of the side sulfonate acid group causes the membrane to degrade thermally.	58
Nafion	Thermal degradation	The effects of cell cold-starting were examined at −5, −10, and −15°C.	The growing volume of ice expansions produced between the membrane and catalyst layer might harm the membrane surface and even cause the catalyst layers to delaminate.	136

as the water content drops.[127] Activation energies for the Grotthus and vehicle mechanisms are currently estimated to be 0.1–0.4 eV (1 eV = 96.5 kJ mol^{-1}) and 0.4–0.9 eV, respectively.[70,128,129]

3.4.2 | Failure mechanism of PEM

Due to the structural, physicochemical, and electrochemical degradation of membranes, membrane failure can result in permanent and long-term performance decline. The development of long-lasting membranes depends on an understanding of these mechanisms of degradation. Chemical, mechanical, and thermal degradation are the three categories into which the most frequent membrane failure mechanisms can be categorized.[130] In Table 2, the most current PEM failure mechanism is summarized. Unfortunately, there is currently a lack of knowledge regarding the mechanisms underlying PEM fuel cell component degradation. In order to do this, a greater focus must be placed on cutting-edge diagnostic techniques and analytical tools.

10974628, 2023, 22, Downloaded from https://onlinelibrary.wiley.com/doi/10.1002/app.53919 by Turkey Cochrane Evidence Aid, Wiley Online Library on [22/05/2025]. See the Terms and Conditions (https://onlinelibrary.wiley.com/terms-and-conditions) on Wiley Online Library for rules of use; OA articles are governed by the applicable Creative Commons License

4 | CONCLUSION AND FUTURE PERSPECTIVE

The PEM with strong proton conductivity and great stability due to chemical structural management, organic–inorganic hybrid composite membrane, and nanofiber composite membrane were summarized in this review. In addition, the presence of an acid-rich layer, acid–base interaction, or strong proton transport channel can be responsible for the proton transport mechanism in PEM. Although the review described recent developments in high-performance PEM fabrication, there are still several unanswered questions. The specifics are discussed below.

Currently, most high-performance PEM achievements have been made in laboratories, making it difficult to overcome the barrier to widespread use in fuel cell applications. Although it is simple to fabricate PEM with various proton conductivities using polymer sulfonation process, the target product with accurate degree of sulfonation is difficult to successfully produce. This issue will worsen and cannot be addressed by practical application in large-scale production. Additionally, although nanoparticles and nanofiber can achieve high-performance levels, large-scale mass production is not possible. The tendency is to construct high-performance PEM with easy fabrication methods, especially raw materials with stable performance.

Consequently, the mechanism is still not deep enough. The existence of an acid-rich layer and acid–base interaction is advantageous for the proton to transport, which can lead to high proton conductivity and stability. However, the size, morphology, and type are not clear yet. Future research may concentrate on a quantitative analysis of the aforementioned mechanism.

Future research must concentrate on simple mass production techniques and quantitative analysis of proton transport mechanisms. Furthermore, nothing is known about the quantitative relationships between the performance degradation brought on by the deterioration of specific fuel cell components. To finally facilitate the transition toward the commercialization of PEM fuel cell technology, it is imperative to make ongoing efforts to propose the appropriate mitigation techniques. These issues necessitate more investigation and rigorous testing because they are essential to achieve ideal performance before the product is actually marketed.

AUTHOR CONTRIBUTIONS

Peng Wei: Conceptualization (lead); investigation (lead); supervision (lead); validation (lead); writing – original draft (lead); writing – review and editing (lead). **Yang Sui:** Writing – original draft (supporting); writing – review and editing (supporting). **Xiaoyu Meng:** Supervision (lead); writing – original draft (supporting); writing – review and editing (supporting).

ACKNOWLEDGMENTS

This project was financially supported by the Foundation of the China University of Petroleum, Beijing (No. 2462020YXZZ019). The China National Key Research and Development Plan (No. 2022YFC2803702).

DATA AVAILABILITY STATEMENT

Research data are not shared.

ORCID

Peng Wei https://orcid.org/0000-0002-4578-449X

REFERENCES

[1] L. Mathur, I.-H. Kim, A. Bhardwaj, B. Singh, J.-Y. Park, S.-J. Song, *Compos. Part B* **2020**, *202*, 108405.
[2] S. J. Peighambardoust, S. Rowshanzamir, M. Amjadi, *Int. J. Hydrog. Energy* **2010**, *35*, 9349.
[3] K. Sopian, W. R. Wan Daud, *Renew. Energy* **2006**, *31*, 719.
[4] W. R. W. Daud, R. E. Rosli, E. H. Majlan, S. A. A. Hamid, R. Mohamed, T. Husaini, *Renew. Energy* **2017**, *113*, 620.
[5] P. Kallem, N. Yanar, H. Choi, *ACS Sustain. Chem. Eng.* **2019**, *7*, 1808.
[6] G. Wang, Y. Yu, H. Liu, C. Gong, S. Wen, X. Wang, Z. Tu, *Fuel Process. Technol.* **2018**, *179*, 203.
[7] X.-Z. Yuan, C. Nayoze-Coynel, N. Shaigan, D. Fisher, N. Zhao, N. Zamel, P. Gazdzicki, M. Ulsh, K. A. Friedrich, F. Girard, U. Groos, *J. Power Sources* **2021**, *491*, 229540.
[8] K. Jiao, J. Xuan, Q. Du, Z. Bao, B. Xie, B. Wang, Y. Zhao, L. Fan, H. Wang, Z. Hou, S. Huo, N. P. Brandon, Y. Yin, M. D. Guiver, *Nature* **2021**, *595*, 361.
[9] J. Mo, Z. Kang, G. Yang, Y. Li, S. T. Retterer, D. A. Cullen, T. J. Toops, G. Bender, B. S. Pivovar, J. B. Green Jr., F.-Y. Zhang, *J. Mater. Chem. A* **2017**, *5*, 18469.
[10] G. Zhao, X. Xu, Y. Di, H. Wang, B. Cheng, L. Shi, Y. Zhu, X. Zhuang, Y. Yin, *J. Power Sources* **2019**, *438*, 227035.
[11] M. Vinothkannan, A. R. Kim, S. Ramakrishnan, Y.-T. Yu, D. J. Yoo, *Compos. Part B* **2021**, *215*, 108828.
[12] A. R. Kim, C. J. Park, M. Vinothkannan, D. J. Yoo, *Compos. Part B* **2018**, *155*, 272.
[13] M. J. Parnian, S. Rowshanzamir, F. Gashoul, *Energy* **2017**, *125*, 614.
[14] C. He, M. D. Guiver, F. Mighri, S. Kaliaguine, *J. Colloid Interface Sci.* **2013**, *409*, 193.
[15] Z. Zhang, J. Ren, J. Xu, Z. Wang, W. He, S. Wang, X. Yang, X. Du, L. Meng, P. Zhao, *J. Membr. Sci.* **2020**, *607*, 118194.
[16] A. Kusoglu, A. Z. Weber, *Chem. Rev.* **2017**, *117*, 987.
[17] K. D. Kreuer, M. Schuster, B. Obliers, O. Diat, U. Traub, A. Fuchs, U. Klock, S. J. Paddison, J. Maier, *J. Power Sources* **2008**, *178*, 499.
[18] D. W. Shin, M. D. Guiver, Y. M. Lee, *Chem. Rev.* **2017**, *117*, 4759.
[19] C. Bi, H. Zhang, S. Xiao, Y. Zhang, Z. Mai, X. Li, *J. Membr. Sci.* **2011**, *376*, 170.

10974628, 2023, 22, Downloaded from https://onlinelibrary.wiley.com/doi/10.1002/app.53919 by Turkey Cochrane Evidence Aid, Wiley Online Library on [22/05/2025]. See the Terms and Conditions (https://onlinelibrary.wiley.com/terms-and-conditions) on Wiley Online Library for rules of use; OA articles are governed by the applicable Creative Commons License

[20] N. Awang, A. F. Ismail, J. Jaafar, T. Matsuura, H. Junoh, M. H. D. Othman, M. A. Rahman, *React. Funct. Polym.* **2015**, *86*, 248.
[21] S. Jang, Y.-G. Yoon, Y.-S. Lee, Y.-W. Choi, *J. Membr. Sci.* **2018**, *563*, 896.
[22] K. Kim, P. Heo, W. Hwang, J. H. Baik, Y. E. Sung, J. C. Lee, *ACS Appl. Mater. Interfaces* **2018**, *10*, 21788.
[23] H. Han, H. Q. Li, M. Liu, L. Xu, J. Xu, S. Wang, H. Ni, Z. Wang, *J. Power Sources* **2017**, *340*, 126.
[24] S.-H. Yun, J.-J. Woo, S.-J. Seo, L. Wu, D. Wu, T. Xu, S.-H. Moon, *J. Membr. Sci.* **2011**, *367*, 296.
[25] X. Li, Y. Song, Z. Liu, P. Feng, S. Liu, Y. Yu, Z. Jiang, B. Liu, *High Perform. Polym.* **2014**, *26*, 106.
[26] J. Han, K. Kim, S. Kim, H. Lee, J. Kim, T. Ko, J. Bae, W. J. Choi, Y.-E. Sung, J.-C. Lee, *J. Power Sources* **2020**, *448*, 227427.
[27] Z. Li, Z. Guan, C. Wang, B. Quan, L. Zhao, *J. Membr. Sci.* **2021**, *620*, 118897.
[28] H. Sun, B. Tang, P. Wu, *ACS Appl. Mater. Interfaces* **2017**, *9*, 26077.
[29] P. Wei, D. Huang, C. Luo, Y. Sui, X. Li, Q. Liu, B. Zhu, C. Cong, Q. Zhou, X. Meng, *Polymer* **2023**, *271*, 125800.
[30] Z. Yin, H. Geng, P. Yang, B. Shi, C. Fan, Q. Peng, H. Wu, Z. Jiang, *Int. J. Hydrog. Energy* **2021**, *46*, 26550.
[31] C. C. Dong, Z. M. Hao, Q. S. Wang, B. S. Zhu, C. B. Cong, X. Y. Meng, Q. Zhou, *Int. J. Hydrog. Energy* **2017**, *42*, 25388.
[32] L. Yu, F. Un, W. Xiao, L. Xu, J. Xi, *Chem. Eng. J.* **2019**, *356*, 622.
[33] X. Li, C. Liu, H. Lu, C. Zhao, Z. Wang, W. Xing, H. Na, *J. Membr. Sci.* **2005**, *255*, 149.
[34] X. Liu, Y. Zhang, S. Deng, C. Li, J. Dong, J. Wang, Z. Yang, D. Wang, H. Cheng, *ACS Appl. Energy Mater.* **2018**, *1*, 5463.
[35] B. Bae, K. Miyatake, M. Watanabe, *Macromolecules* **2009**, *42*, 1873.
[36] K. Miyatake, Y. Chikashige, E. Higuchi, M. Watanabe, *J. Am. Chem. Soc.* **2007**, *129*, 3879.
[37] C. Ni, Y. Wei, Q. Hu, X. Li, B. Liu, Q. Zhao, M. Zhang, Y. Li, W. Hu, *Solid State Ionics* **2016**, *297*, 29.
[38] J. Wang, J. Lin, Z. Zhou, Y. Zhang, Z. Yang, W. Wu, *J. Membr. Sci.* **2021**, *640*, 119818.
[39] A. S. Badami, O. Lane, H.-S. Lee, A. Roy, J. E. McGrath, *J. Membr. Sci.* **2009**, *333*, 1.
[40] X. Yu, A. Roy, S. Dunn, A. S. Badami, J. Yang, A. S. Good, J. E. McGrath, *J. Polym. Sci. Part A: Polym. Chem.* **2009**, *47*, 1038.
[41] N. Li, C. Wang, S. Y. Lee, C. H. Park, Y. M. Lee, M. D. Guiver, *Angew. Chem. Int. Ed.* **2011**, *50*, 9158.
[42] L. Li, J. Zhang, Y. X. Wang, *J. Membr. Sci.* **2003**, *226*, 159.
[43] P. X. Xing, G. P. Robertson, M. D. Guiver, S. D. Mikhailenko, K. P. Wang, S. Kaliaguine, *J. Membr. Sci.* **2004**, *229*, 95.
[44] Z. Yuan, L. Liang, Q. Dai, T. Li, Q. Song, H. Zhang, G. Hou, X. Li, *Joule* **2022**, *6*, 884.
[45] B. P. Tripathi, V. K. Shahi, *Prog. Polym. Sci.* **2011**, *36*, 945.
[46] K. Ketpang, B. Son, D. Lee, S. Shanmugam, *J. Membr. Sci.* **2015**, *488*, 154.
[47] T. Kasuga, *Thin Solid Films* **2006**, *496*, 141.
[48] S. Zhao, J. Ren, Y. Wang, J. Zhang, *J. Membr. Sci.* **2013**, *437*, 65.
[49] K. Ketpang, S. Shanmugam, C. Suwanboon, N. Chanunpanich, D. Lee, *J. Membr. Sci.* **2015**, *493*, 285.
[50] A. Ortiz-Negron, D. Suleiman, *J. Appl. Polym. Sci.* **2015**, *132*, 42651.
[51] J. Zhao, D. Song, J. Jia, N. Wang, K. Liu, T. Zuo, Q. Che, *Appl. Surf. Sci.* **2022**, *585*, 152579.
[52] B. B. Munavalli, S. N. Hegde, M. Y. Kariduraganavar, *J. Appl. Polym. Sci.* **2022**, *139*, e52388.
[53] C. Dong, Q. Wang, C. Cong, X. Meng, Q. Zhou, *Int. J. Hydrog. Energy* **2017**, *42*, 10317.
[54] C. Dong, Z. Shi, Q. Zhou, *J. Appl. Polym. Sci.* **2020**, *137*, e49388.
[55] B. R. Matos, E. I. Santiago, J. F. Q. Rey, A. S. Ferlauto, E. Traversa, M. Linardi, F. C. Fonseca, *J. Power Sources* **2011**, *196*, 1061.
[56] H. Gao, C. Dong, Q. Wang, H. Zhu, X. Meng, C. Cong, Q. Zhou, *Int. J. Hydrog. Energy* **2018**, *43*, 21940.
[57] X. Meng, C. Li, J. Wen, H. Ye, C. Cong, Q. Zhou, L. Xu, *J. Chin. Chem. Soc.* **2021**, *68*, 1197.
[58] Z. Zhang, J. Ren, J. Xu, L. Meng, P. Zhao, H. Wang, Z. Wang, *J. Membr. Sci.* **2021**, *630*, 119304.
[59] C. Gong, H. Liu, B. Zhang, G. Wang, F. Cheng, G. Zheng, S. Wen, Z. Xue, X. Xie, *J. Membr. Sci.* **2017**, *535*, 113.
[60] S. Lu, D. Wang, S. P. Jiang, Y. Xiang, J. Lu, J. Zeng, *Adv. Mater.* **2010**, *22*, 971.
[61] A. R. Motz, M.-C. Kuo, J. L. Horan, R. Yadav, S. Seifert, T. P. Pandey, S. Galioto, Y. Yang, N. V. Dale, S. J. Hamrock, A. M. Herring, *Energy Environ. Sci.* **2018**, *11*, 1499.
[62] E. Fontananova, F. Trotta, J. C. Jansen, E. Drioli, *J. Membr. Sci.* **2010**, *348*, 326.
[63] H. Wu, X. Shen, Y. Cao, Z. Li, Z. Jiang, *J. Membr. Sci.* **2014**, *451*, 74.
[64] J. L. Lu, Q. H. Fang, S. L. Li, S. P. Jiang, *J. Membr. Sci.* **2013**, *427*, 101.
[65] S. Zhai, H. Song, X. Jia, K. Yang, M. Feng, S. He, J. Lin, *J. Power Sources* **2021**, *506*, 230195.
[66] L. Yang, B. Tang, P. Wu, *J. Mater. Chem. A* **2015**, *3*, 15838.
[67] Y. Y. Cai, Q. Yang, Z. Y. Zhu, Q. H. Sun, A. M. Zhu, Q. G. Zhang, Q. L. Liu, *J. Membr. Sci.* **2019**, *590*, 117277.
[68] H. S. Sasmal, H. B. Aiyappa, S. N. Bhange, S. Karak, A. Halder, S. Kurungot, R. Banerjee, *Angew. Chem. Int. Ed.* **2018**, *130*, 11060.
[69] P. Li, J. Chen, S. K. Tang, *Chem. Eng. J.* **2021**, *415*, 129021.
[70] S. Chen, Y. Wu, Y. Zhang, W. Zhang, Y. Fu, W. Huang, T. Yan, H. Ma, *J. Mater. Chem. A* **2020**, *8*, 13702.
[71] Y. Yin, H. Wang, L. Cao, Z. Li, Z. Li, M. Gang, C. Wang, H. Wu, Z. Jiang, P. Zhang, *Electrochim. Acta* **2016**, *203*, 178.
[72] C. Simari, E. Lufrano, A. Brunetti, G. Barbieri, I. Nicotera, *Electrochim. Acta* **2021**, *380*, 138214.
[73] Y. C. Chen, A. Y. Lu, P. Lu, X. Yang, C. M. Jiang, M. Mariano, B. Kaehr, O. Lin, A. Taylor, I. D. Sharp, L. J. Li, S. S. Chou, V. Tung, *Adv. Mater.* **2017**, *29*, 201703863.
[74] K. Divya, M. S. S. A. Saraswathi, D. Rana, S. Alwarappan, A. Nagendran, *Polymer* **2018**, *147*, 48.
[75] Y. Shi, S. Jiang, K. Zhou, C. Bao, B. Yu, X. Qian, B. Wang, N. Hong, P. Wen, Z. Gui, Y. Hu, R. K. K. Yuen, *ACS Appl. Mater. Interfaces* **2014**, *6*, 429.
[76] M. Gang, G. He, Z. Li, K. Cao, Z. Li, Y. Yin, H. Wu, Z. Jiang, *J. Membr. Sci.* **2016**, *507*, 1.
[77] R. T. Niu, L. Q. Kong, L. Y. Zheng, H. X. Wang, H. F. Shi, *J. Membr. Sci.* **2017**, *525*, 220.
[78] Y. Wang, L. Liu, Y. Liu, N. Li, Z. Hu, S. Chen, *Polymer* **2022**, *238*, 124426.
[79] Y. Ye, L. Gong, S. Xiang, Z. Zhang, B. Chen, *Adv. Mater.* **2020**, *32*, 1907090.

10974628, 2023, 22, Downloaded from https://onlinelibrary.wiley.com/doi/10.1002/app.53919 by Turkey Cochrane Evidence Aid, Wiley Online Library on [23/05/2025]. See the Terms and Conditions (https://onlinelibrary.wiley.com/terms-and-conditions) on Wiley Online Library for rules of use; OA articles are governed by the applicable Creative Commons License

[80] L. Wang, N. Deng, G. Wang, J. Ju, B. Cheng, W. Kang, *ACS Appl. Mater. Interfaces* **2019**, *11*, 39979.
[81] S. He, S. Liu, W. Dai, S. Zhai, J. Lin, *J. Electrochem. Soc.* **2018**, *165*, F951.
[82] H. Z. Sun, B. B. Tang, P. Y. Wu, *ACS Appl. Mater. Interfaces* **2017**, *9*, 35075.
[83] B. Zhang, Y. Cao, Z. Li, H. Wu, Y. Yin, L. Cao, X. He, Z. Jiang, *Electrochim. Acta* **2017**, *240*, 186.
[84] S. Gahlot, V. Kulshrestha, *ACS Appl. Mater. Interfaces* **2015**, *7*, 264.
[85] F. F. Fang, L. Liu, L. F. Min, L. Xu, W. Zhang, Y. X. Wang, *Int. J. Hydrog. Energy* **2021**, *46*, 17784.
[86] X. Liu, J. F. Zhang, C. Y. Zheng, J. D. Xue, T. Huang, Y. Yin, Y. Z. Qin, K. Jiao, Q. Du, M. D. Guiver, *Energy Environ. Sci.* **2020**, *13*, 297.
[87] X. Liu, Y. Li, J. D. Xue, W. K. Zhu, J. F. Zhang, Y. Yin, Y. Z. Qin, K. Jiao, Q. Du, B. W. Cheng, X. P. Zhuang, J. X. Li, M. D. Guiver, *Nat. Commun.* **2019**, *10*, 842.
[88] L. Liu, X. Li, Z. Liu, S. Zhang, L. Qian, Z. Chen, J. Li, P. Fang, C. He, *J. Membr. Sci.* **2022**, *653*, 120516.
[89] K. Pourzare, Y. Mansourpanah, S. Farhadi, M. M. H. Sadrabadi, I. Frost, M. Ulbricht, *Solid State Ionics* **2020**, *351*, 115343.
[90] P. Wei, Y. Sui, X. Li, Q. Liu, B. Zhu, C. Cong, X. Meng, Q. Zhou, *J. Membr. Sci.* **2022**, *644*, 120116.
[91] P. Wei, D. Huang, X. Li, B. Zhu, C. Cong, X. Meng, Q. Zhou, J. Phys, *Conf. Ser.* **2022**, *2194*, 012003.
[92] R. Sood, S. Cavaliere, D. J. Jones, J. Roziere, *Nano Energy* **2016**, *26*, 729.
[93] L. Wang, X. Zuo, A. Raut, R. Isseroff, Y. Xue, Y. Zhou, B. Sandhu, T. Schein, T. Zeliznyak, P. Sharma, S. Sharma, B. S. Hsiao, M. H. Rafailovich, *Sustain. Energy Fuels* **2019**, *3*, 2725.
[94] S. Zhang, G. He, X. Gong, X. Zhu, X. Wu, X. Sun, X. Zhao, H. Li, *J. Membr. Sci.* **2015**, *493*, 58.
[95] D. Li, Y. N. Xia, *Adv. Mater.* **2004**, *16*, 1151.
[96] A. Greiner, J. H. Wendorff, *Angew. Chem. Int. Ed.* **2007**, *46*, 5670.
[97] J. Wang, P. Li, Y. Zhang, Y. Liu, W. Wu, J. Liu, *J. Membr. Sci.* **2019**, *585*, 157.
[98] D. Powers, R. Wycisk, P. N. Pintauro, *J. Membr. Sci.* **2019**, *573*, 107.
[99] D. S. Liu, J. N. Ashcraft, M. M. Mannarino, M. N. Silberstein, A. A. Argun, G. C. Rutledge, M. C. Boyce, P. T. Hammond, *Adv. Funct. Mater.* **2013**, *23*, 3087.
[100] M. M. Mannarino, D. S. Liu, P. T. Hammond, G. C. Rutledge, *ACS Appl. Mater. Interfaces* **2013**, *5*, 8155.
[101] J. W. Park, R. Wycisk, P. N. Pintauro, *J. Membr. Sci.* **2015**, *490*, 103.
[102] M. Oroujzadeh, S. Mehdipour-Ataei, M. Esfandeh, *Chem. Eng. J.* **2015**, *269*, 212.
[103] Q. Yuan, Z. Fu, Y. Wang, W. Chen, X. Wu, X. Gong, D. Zhen, X. Jian, G. He, *J. Membr. Sci.* **2020**, *595*, 117516.
[104] Y. Wu, G. He, X. Wu, Q. Yuan, X. Gong, D. Zhen, B. Sun, *Int. J. Hydrog. Energy* **2019**, *44*, 7494.
[105] B. Zhu, Y. Sui, P. Wei, J. Wen, H. Cao, C. Cong, X. Meng, Q. Zhou, *J. Membr. Sci.* **2021**, *628*, 119214.
[106] D. Huang, X. Li, C. Luo, P. Wei, Y. Sui, J. Wen, C. Cong, X. Zhang, X. Meng, Q. Zhou, *J. Membr. Sci.* **2022**, *662*, 121001.
[107] Y. Li, J. Hui, J. Kawchuk, A. O'Brien, Z. Jiang, M. Hoorfar, *Fuel Cells* **2019**, *19*, 43.
[108] G. L. Liu, W. C. Tsen, S. C. Jang, F. Q. Hu, F. Zhong, H. Liu, G. J. Wang, S. Wen, G. W. Zheng, C. L. Gong, *J. Membr. Sci.* **2019**, *591*, 117321.
[109] G. Zhao, X. Xu, H. Zhao, L. Shi, X. Zhuang, B. Cheng, Y. Yin, *J. Membr. Sci.* **2020**, *601*, 117914.
[110] T. Makinouchi, M. Tanaka, H. Kawakami, *J. Membr. Sci.* **2017**, *530*, 65.
[111] Y. Yao, Z. Lin, Y. Li, M. Alcoutlabi, H. Hamouda, X. Zhang, *Adv. Energy Mater.* **2011**, *1*, 1133.
[112] M. Tanaka, Y. Takeda, T. Wakiya, Y. Wakamoto, K. Harigaya, T. Ito, T. Tarao, H. Kawakami, *J. Power Sources* **2017**, *342*, 125.
[113] X. Gong, G. He, Y. Wu, S. Zhang, B. Chen, Y. Dai, X. Wu, *J. Power Sources* **2017**, *358*, 134.
[114] T. Ogawa, T. Aonuma, T. Tamaki, H. Ohashi, H. Ushiyama, K. Yamashita, T. Yamaguchi, *Chem. Sci.* **2014**, *5*, 4878.
[115] Y. He, H. Zhang, Y. Li, J. Wang, L. Ma, W. Zhang, J. Liu, *J. Mater. Chem. A* **2015**, *3*, 21832.
[116] J. Wang, Y. He, L. Zhao, Y. Li, S. Cao, B. Zhang, H. Zhang, *J. Membr. Sci.* **2015**, *482*, 1.
[117] G. Zhao, X. Xu, L. Shi, B. Cheng, X. Zhuang, Y. Yin, *J. Power Sources* **2020**, *452*, 227839.
[118] S. Gao, H. Xu, Z. Fang, A. Ouadah, H. Chen, X. Chen, L. Shi, B. Ma, C. Jing, C. Zhu, *Electrochim. Acta* **2018**, *283*, 428.
[119] X. Wu, X. Wang, G. He, J. Benziger, *J. Polym. Sci. B Polym. Phys.* **2011**, *49*, 1437.
[120] K. Schmidt-Rohr, Q. Chen, *Nat. Mater.* **2008**, *7*, 75.
[121] G. Gebel, *Macromolecules* **2013**, *46*, 6057.
[122] T. J. Peckham, S. Holdcroft, *Adv. Mater.* **2010**, *22*, 4667.
[123] P. Choi, N. H. Jalani, R. Datta, *J. Electrochem. Soc.* **2005**, *152*, E123.
[124] K. D. Kreuer, A. Rabenau, W. Weppner, *Angew. Chem. Int. Ed.* **1982**, *21*, 208.
[125] N. Agmon, *Chem. Phys. Lett.* **1995**, *244*, 456.
[126] M. Eikerling, A. A. Kornyshev, *J. Electroanal. Chem.* **2001**, *502*, 1.
[127] M. Eikerling, A. A. Kornyshev, A. M. Kuznetsov, J. Ulstrup, S. Walbran, *J. Phys. Chem. B* **2001**, *105*, 3646.
[128] P. Ramaswamy, N. E. Wong, G. K. H. Shimizu, *Chem. Soc. Rev.* **2014**, *43*, 5913.
[129] Y. Yin, W. Deng, H. Wang, A. Li, C. Wang, Z. Jiang, H. Wu, *J. Mater. Chem. A* **2015**, *3*, 16079.
[130] M. Pan, C. Pan, C. Li, J. Zhao, *Renew. Sust. Energ. Rev.* **2021**, *141*, 110771.
[131] J. Peng, X. Fu, J. Luo, L. Wang, X. Peng, *Chem. Eng. J.* **2023**, *453*, 139609.
[132] W. Yu, Z. Ge, K. Zhang, X. Liang, X. Ge, H. Wang, M. Li, X. Shen, Y. Xu, L. Wu, T. Xu, *Ind. Eng. Chem. Res.* **2022**, *61*, 4329.
[133] R. M. H. Khorasany, A. Sadeghi Alavijeh, E. Kjeang, G. G. Wang, R. K. N. D. Rajapakse, *J. Power Sources* **2015**, *274*, 1208.
[134] Y. Singh, R. T. White, M. Najm, T. Haddow, V. Pan, F. P. Orfino, M. Dutta, E. Kjeang, *J. Power Sources* **2019**, *412*, 224.
[135] R. M. H. Khorasany, E. Kjeang, G. G. Wang, R. K. N. D. Rajapakse, *J. Power Sources* **2015**, *279*, 55.
[136] Q. Yan, H. Toghiani, Y.-W. Lee, K. Liang, H. Causey, *J. Power Sources* **2006**, *160*, 1242.

10974628, 2023, 22, Downloaded from https://onlinelibrary.wiley.com/doi/10.1002/app.53919 by Turkey Cochrane Evidence Aid, Wiley Online Library on [22/05/2025]. See the Terms and Conditions (https://onlinelibrary.wiley.com/terms-and-conditions) on Wiley Online Library for rules of use; OA articles are governed by the applicable Creative Commons License

AUTHOR BIOGRAPHIES



Peng Wei obtained his Doctor Degree in Material Science and Engineering from China University of Petroleum-Beijing in June 2022 and now he is assistant research at Tsinghua University. His current study focuses primarily on polymer friction and proton exchange membrane and has published 4 patents and 10 peer-reviewed articles.



Yang Sui obtained her Master Degree in Materials Science from Washington University in St. Louis (WUSTL) in August 2020 and now is a PhD candidate of China University of Petroleum (Beijing) under the supervision of professor Qiong Zhou. Her current research interests mainly focus on rheological behavior and application of polymer nanocomposites.



Xiaoyu Meng is a deputy director of Beijing Key Laboratory of Oil and Gas Equipment Material Failure and Corrosion Protection and an Associate Professor at the China University of Petroleum-Beijing. His work concentrates on fabricating high-performance proton exchange membranes for fuel cells and the high performance of polymer and its application in the petroleum industry.



Qiong Zhou is the director of the Nonmetallic Materials Laboratory for Energy Equipment and a full professor at the China University of Petroleum-Beijing. Her work concentrates on the use of high-performance polymers in the energy sector, proton exchange membranes for fuel cells, corrosion-resistant materials for high-sulfur environments, and other topics. The research on the preparation and application of polymer nanocomposites has achieved great progress. She has 12 patents and more than 100 peer-reviewed articles published.

How to cite this article: P. Wei, Y. Sui, X. Meng, Q. Zhou, *J. Appl. Polym. Sci.* **2023**, *140*(22), e53919. https://doi.org/10.1002/app.53919

10974628, 2023, 22, Downloaded from https://onlinelibrary.wiley.com/doi/10.1002/app.53919 by Turkey Cochrane Evidence Aid, Wiley Online Library on [23/05/2025]. See the Terms and Conditions (https://onlinelibrary.wiley.com/terms-and-conditions) on Wiley Online Library for rules of use; OA articles are governed by the applicable Creative Commons License